JOM Journal of Optical Microsystems

REVIEW

Emulating paper: a review of reflective display technologies

Dorian Herle[a,*] **Olivier J. F. Martin**[b] **Luis Guillermo Villanueva**[a] **and Niels Quack**[c,*]

[a]Ecole Polytechnique Fédérale de Lausanne, Advanced Nano-Mechanical Systems Laboratory, Lausanne, Switzerland

[b]Ecole Polytechnique Fédérale de Lausanne, Nanophotonics and Metrology Laboratory, Lausanne, Switzerland

[c]The University of Sydney, Micro- and Nanosystems, Sydney, New South Wales, Australia

ABSTRACT. Reflective displays, which harness ambient light, offer energy-efficient alternatives to traditional emissive screens in mobile devices. This review provides an overview of various reflective display technologies and their comparative performance metrics. The review highlights the potential of micro-electromechanical system-based displays, with metrics including 90% reflectance, a contrast ratio of 30, a frequency of 120 Hz, and a resolution of about 350 pixels per inch. Their applicability to mainstream devices such as e-readers, smartphones, and smartwatches continues to be a topic of interest and exploration.

Keywords: reflective displays; mobile devices; ambient light; optics; light modulators

Paper 23034V received Oct. 13, 2023; revised Mar. 10, 2024; accepted Mar. 18, 2024; published Apr. 11, 2024.

1 Introduction

The swift evolution of the internet, digital data, and entertainment, coupled with the rise in a plethora of applications, has made electronic displays a crucial daily necessity. Since the introduction of liquid-crystal displays (LCDs) in 1968 by George Heilmeier of RCA,[1] display technologies have shown significant advancements, resulting in images with exceptional color reproduction and unprecedented sharpness. Recent reviews have focused on emissive display technologies, including LC, organic light-emitting diode (OLED), mini- and micro-LED emissive displays,[2,3] and quantum dot displays.[4]

Moreover, a critical review published in 2011 highlighted the present and future prospects of electronic paper, detailing the performance limitations and possible future breakthroughs.[5] Fast forward to the present, a recent book on E-paper displays underscores the growing importance of this technology, emphasizing its low power consumption and potential for reducing eye strain.[6]

As electronic displays have become increasingly portable and widespread, the expectations and demands on their performance have also grown. In particular, the need for increased battery life and optimal visibility in various lighting conditions are critical for modern mobile devices. Emissive display technologies need to generate enough light to adapt to the ambient light levels. As human eyes adjust to the surrounding brightness, these technologies can lead to a perceived decrease in contrast ratio (CR) in areas with ample lighting. Unfortunately, increasing the emissivity of a display to align with the lighting conditions also results in increased energy consumption.

*Address all correspondence to Dorian Herle, dorian.herle@epfl.ch; Niels Quack, niels.quack@sydney.edu.au

This oxymoron of the emissive display can partly be lessened by the utilization of more efficient light generation, such as OLED and micro-LED technology, yet it remains an inevitable challenge. Reflective displays on the other hand provide a more elegant and natural solution. Similar to any printed medium, this technology does not need to emit light. Instead, ambient light is utilized to show the image. The benefits are directly apparent: perfect readability in bright environments, while being more energy efficient than their emissive counterparts. Readability in darkness is usually achieved by an integrated front light.

Throughout the years, a plethora of reflective display technologies have been invented and researched; these include electrowetting, reflective LC, electrochromic, micro-electromechanical systems (MEMS), tunable photonic crystals, and electrophoretic displays. Each technology has its own set of benefits and drawbacks in terms of peak reflectivity, CR, achievable frequency, and resolution, as well as power consumption.

Understanding the fundamental concepts, performance, and prospective uses of these display technologies is becoming increasingly important as the field advances and diversifies. In this review article, we provide a comprehensive overview of various reflective display technologies, highlighting their key features, operation mechanisms, and recent advances in the field. Our aim is to offer a valuable resource for those interested in the current state of the art and the future direction of electronic display research and development, particularly for low-power mobile devices. To facilitate a deeper understanding, the review is organized into several sections, each dedicated to a specific technology. Each section delves into the origin, working principles, commercial applications, and challenges associated with the respective technology. The aim of this structured approach is to offer a valuable resource for readers interested in the current state of the art as well as the future direction of electronic display research and development.

2 Print Media as Benchmark for Reflective Displays

A commonly employed benchmark for assessing the static performance of reflective displays is the extent to which they can emulate the visual characteristics of traditional print media. These characteristics include elements such as ambient CR, white state reflectivity, color, and bistability. These benchmarks serve to gauge the performance of reflective displays, while aligning with foundational measurement parameters highlighted in the broader context of display technologies.[7] By focusing on these four key characteristics, this chapter aims to offer a comprehensive understanding of how reflective displays measure up to print media in terms of readability and visual comfort.

2.1 Ambient Contrast Ratio

White paper can be described as a close approximation of a perfectly diffuse, or Lambertian, surface,[8] making it appear bright from any viewing angle. At the same time, black pigments absorb most of the light. The ratio between the brightest and darkest state is commonly referred to as "contrast" or CR. Although emissive displays frequently exhibit exceedingly high CRs, it is important to note that these values are typically attained under dark environmental conditions. Under bright ambient conditions these values usually greatly deteriorate for emissive displays, as can be seen in Fig. 1.

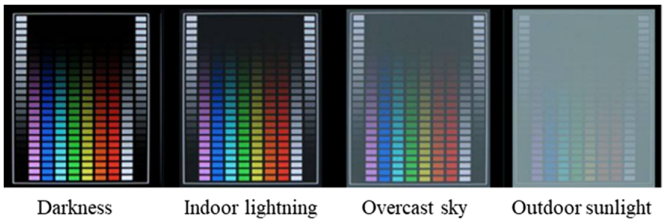

Fig. 1 Qualitative photographs of a representative emissive display under different ambient conditions. Photographs are taken in darkness (0 lux), indoor lighting (1k lux), overcast sky (5k lux), and outdoor sunlight (40k lux). Adapted with permission from Ref. 9, copyright (2021), DisplayMate Technologies.

The ambient CR (ACR), as defined in Eq. (1), offers a more accurate approach for evaluating display performance, particularly for reflective displays, as it takes into consideration the real-world lighting conditions in which these devices operate:[10]

$$\mathrm{ACR} = \frac{L_{\mathrm{on}} + L_{\mathrm{Ambient}} R_L}{L_{\mathrm{off}} + L_{\mathrm{Ambient}} R_L}, \tag{1}$$

where L_{on} and L_{off} are the display's "on" and "off" luminance, respectively, L_{Ambient} is the ambient light, and R_L is the display's luminous reflectance.[11] The latter quantifies the amount of visible light reflected by a display panel under ambient lighting conditions, considering the human eye sensitivity $V(\lambda)$ (i.e., CIE 2° Standard Observer), the spectrum of the incident ambient light $\mathrm{S}(\lambda)$ (i.e., CIE standard D65 light source), and the spectral reflectance of the display $R(\lambda)$. Mathematically, it is defined as follows:

$$R_L = \frac{\int_{\lambda_1}^{\lambda_2} V(\lambda) S(\lambda) R(\lambda) \mathrm{d}\lambda}{\int_{\lambda_1}^{\lambda_2} V(\lambda) S(\lambda) \mathrm{d}\lambda}. \tag{2}$$

R_L serves as an index for evaluating the undesirable reflection of environmental light, which could compromise the legibility and visual comfort of the display interface. Using Eq. (1), with an average R_L of 4% and a typical portable display luminance of 1500 lux, the ambient CR drops to below 2 in direct sunlight (40 K lux), which renders the screen illegible. Table 1 describes human readability within terms of ACR.

2.2 White State Reflectivity

Next to ACR, white state reflectivity is important for mimicking the appearance of paper. Figure 2 compares the black and white reflectance of three different media: high-quality glossy print, standard print, and LCDs. As can be seen, glossy prints have a white state reflectivity of around 80%, which sets them apart from the average 30% reflectivity found in reflective LCDs.

2.3 Color

Color reflective displays pose another layer of difficulty in obtaining bright vivid colors. Much of it boils down to the right color system choice, of which a few prominent once are displayed in Fig. 3. Emissive displays predominantly employ an RGB (red-green-blue) system or an augmented RGBW (red-green-blue-white) system. In the context of reflective displays, using an RGB system leads to a maximum white-state reflectance of 33%, as each subpixel in an RGB configuration only contributes 33% of the light. Similarly, an RGBW system can achieve a maximum white-state reflectance of 50% due to the added white subpixel, which further contributes to the overall reflectance. These values assume fully saturated color filters and are usually lower in practice.

Subtractive color systems, such as CMY (cyan-magenta-yellow) and CMYK (cyan-magenta-yellow-black), have traditionally been used in the printing industry and usually employ a stacked architecture that greatly enhances light conversion. An optimal white state and maximum color fraction, defined as the effective area over which saturated color can be displayed,[5]

Table 1 Ambient CR and readability.

Ambient contrast ratio	Readability
1-2	Illegible under direct sunlight
3-4	Sufficient readability in shade; marginal legibility under direct sunlight
5-9	Adequate readability in sunlight; satisfactory appearance
10	Highly legible in sunlight; visually appealing
15	Exceptional readability; aesthetically pleasing
20	Superior performance; outstanding readability

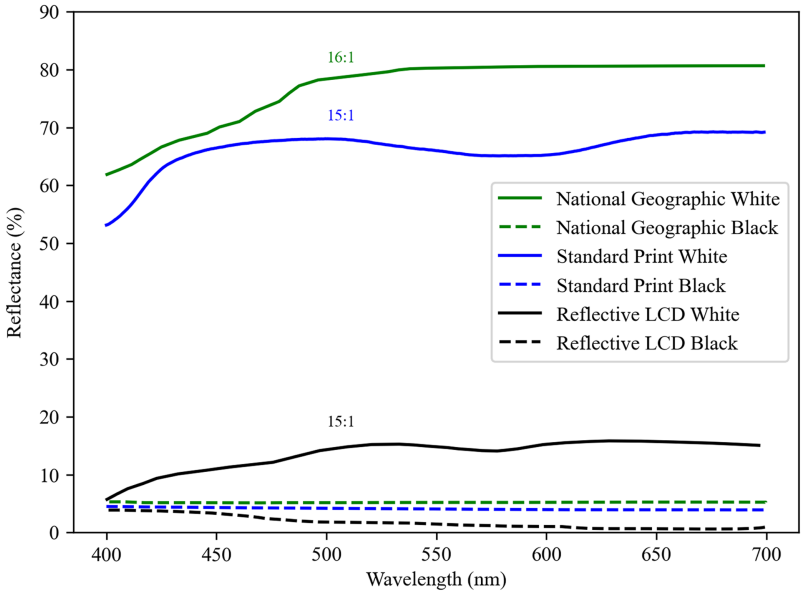

Fig. 2 Reflectance spectra for white and black states of a high-quality magazine print (National Geographic), standard print, and a reflective LCD. CRs are indicated on top of the white reflectance lines. Data for Reflective LCD and National Geographic are sourced from Ref. 12.

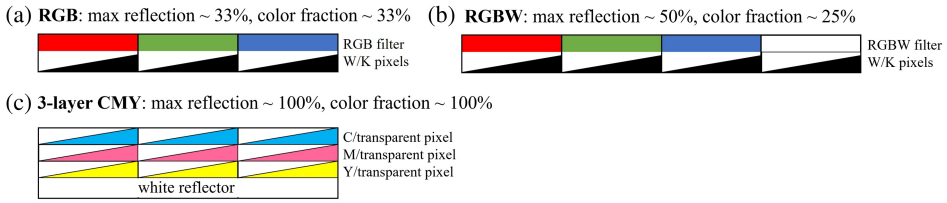

Fig. 3 Schematic representation of different color systems. (a) Red-green-blue (RGB) color filters on top of white-black switching pixels, results in a maximum reflection of 33% and a color fraction (the effective area over which saturated color can be displayed) of 33%' (b) red-green-blue-white (RGBW) color filters add an additional white filter, increasing maximum reflection to 50%, although at the cost of a reduced color fraction of 25%; and (c) three-layer cyan-magenta-yellow pixels with a white reflector yield an exceptional maximum reflection and a color fraction of 100%. This configuration is mostly used in print media. Adapted with permission from Ref. 5, copyright (2011), Society for Information Display.

can be realized through the incorporation of a tri-layered structure featuring CMY (cyan-magenta-yellow) switching layers in the display system.[13,14] At the same time, stacked displays increase costs and complexity because they require more materials, additional backplanes, and complex driving electronics. In addition, the pixel resolution must be limited to maintain enough clear aperture, which helps reduce optical losses and parallax problems. To avoid significant parallax issues, the distance between the front and rear pixels in a multi-layer stack should not be larger than the pixel size itself. This becomes challenging when dealing with very high-resolution displays. It is clear that subpixels capable of transitioning among multiple color states, surpassing the conventional binary (on/off) color limitation, offer the potential to develop single-layered display systems capable of achieving 100% color reproduction.[5]

2.4 Bistability

Once printed on paper, no further energy is required to see the image or text. Ideally, this should be mimicked in reflective display technology. Bistability, a desirable feature for display devices, refers to the ability to maintain image persistence in two stable states without requiring continuous energy. This means that once the image or text is printed, it can be seen without the need for additional energy.

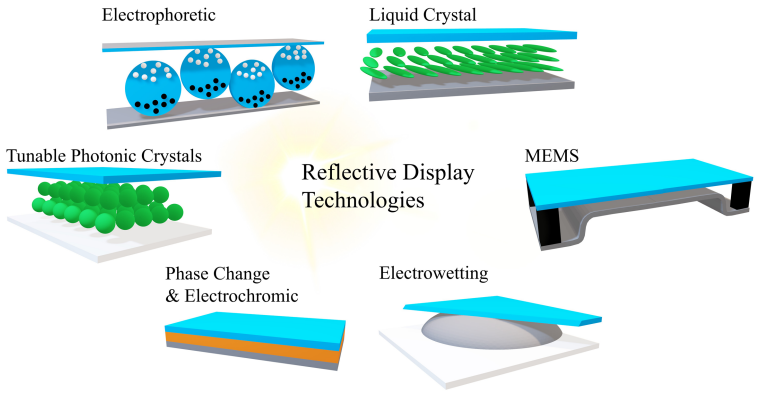

Fig. 4 Schematic visualization of the discussed reflective display technologies. Light manipulation principles across these display technologies: LCDs – polarization, MEMS (IMOD) - interference, electrowetting and electrophoretic - absorptive media transport, phase-change - refractive index, electrochromic - band-gap adjustment, and photonic crystals - diffraction.

3 Reflective Display Technologies

Reflective displays technologies have been evolving since the 1970s, with the introduction of "Gyricon" at Xerox's Palo Alto Research Center [12]. Over the years, numerous e-paper technologies have been developed, and they can be broadly classified based on their tunability mechanisms. These categories are shown in Fig. 4 and encompass electrophoretic, LCs, MEMS, electrowetting, phase change, electrochromic, and tunable photonic crystals.

In the following sections, we delve into each actuation mechanism, discussing the fundamental principles, implementations, and possible outlook. By examining these technologies in detail, we aim to provide a comprehensive understanding of the diverse e-paper landscape and its ongoing developments.

4 Electrophoretic

Electrophoresis describes the motion of charged particles relative to a fluid under the influence of an external electric field. Although the beginning of electrophoretic displays can be attributed to the printing company Xerox, which was granted a patent on "color display device" in 1971,[15] it was the introduction of microencapsulation of the charged particles by Comiskey et al.[16] from MIT that allowed this technology to mature to commercial readiness, resulting in the creation of the commercial entity EInk. Despite its progress, the lack of video compatibility in electrophoretic displays is a significant challenge for widespread adoption in mobile devices. This limitation triggered the exploration of innovative solutions, one of which has been the employment of total internal reflection (TIR) modulation, allowing for a much-reduced particle traveling distance. The electrophoretic TIR display has been commercialized by the company "CLEARink Displays, Inc." short for "charged liquid electro-active response." CLEARink Displays emerged as a separate entity from the University of British Columbia in 2012.[17] Both technologies are presented in the following sections.

4.1 Working Principle

In general, an electrophoretic display operates by displacing charged pigments in and out of sight using electrostatic fields. Equation (3) describes the particle velocity (with initial condition $v_0 = 0$). The formula is derived by equating the electric attraction forces acting on a charged particle due to an external electric field with the fluidic drag forces counteracting the particle mobility, which are given by Stoke's law as[18]

$$v = \frac{qE}{6\pi\mu d}\left(1 - e^{-\frac{6\pi\mu d}{m}t}\right), \tag{3}$$

where v is the particle velocity, E is the applied electric field, q_P is the particle charge, μ is the fluid's viscosity, d is the particle's diameter, and m is the mass of the particle.

As can be observed from Eq. (3), the particle velocity, and thus the speed at which a single pixel can switch states, is influenced by several factors. One of the key determinants is the particle charge. It is most often deduced from the Zeta potential, which is a measure of the electrostatic potential difference between the fluid and the outer layer of the electrical double layer surrounding the particle. This parameter provides a nuanced measure of the particle's effective charge and its interactions with the fluid. For low-dielectric media, it is proportional to the particle charge.[19] A high absolute value of the Zeta potential ensures better dispersion of the particles, reducing aggregation and enhancing the display's long-term reliability. Separately, it is important to note the limitations imposed by the applied electric field. Research efforts have been focused on reducing the required traveling distance, reducing the electrode spacing, and improving the chemical properties of the system.

4.2 Implementations

Microcapsule electrophoretic displays utilize electric fields to move highly scattering or absorbing microparticles vertically within a microcapsule. A multitude of these microcapsules forms one pixel, and monochrome or color systems can be developed.

4.2.1 *Monochrome system*

To this date, vertical dual-particle electrophoretic-based displays have been the most commercially successful reflective display technology on the market. As can be seen in Fig. 5, depending on the applied electric field, different colored particles with either positive or negative zeta potential are selectively moved to the surface, creating the desired image or text.

White particles often consist of inorganic pigments, such as TiO_2, ZrO_2, ZnO, or Al_2O_3, and black particles are often made from Color Index black pigments, iron oxide, or carbon black.[22] These particles are dispersed in a non-polar fluid, which helps reduce leakage currents within the display. Surfactants are added into the system to prevent particle agglomeration[23] and to aid particle charging.[24] To reduce the switching voltage, a specialized coating formulation is

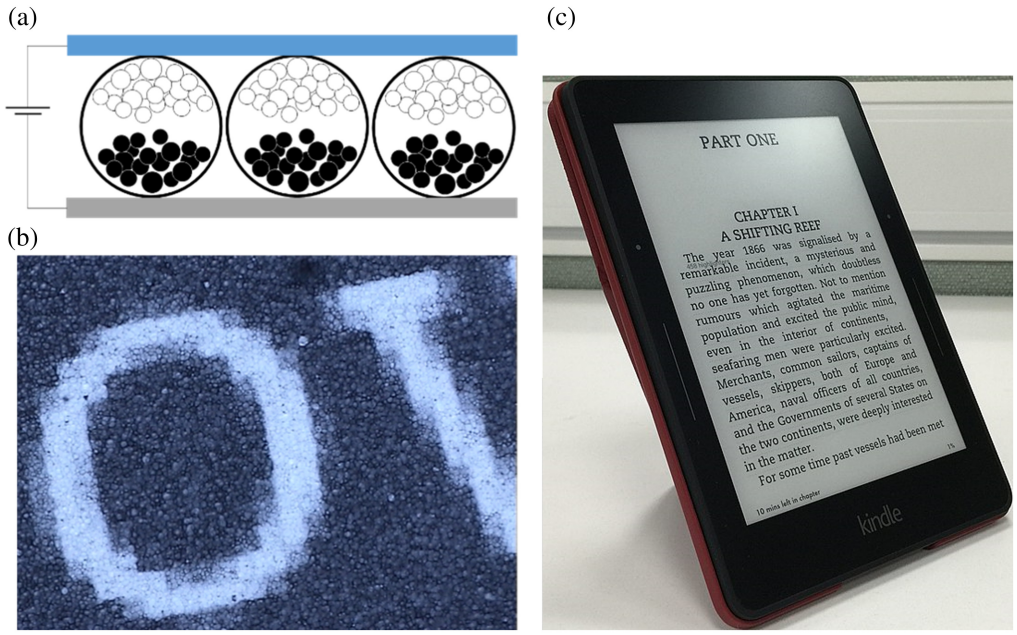

Fig. 5 Microcapsule electrophoretic display. (a) Schematic representation of an electrophoretic microencapsulated black and white ink, wherein the displayed color is controlled by the polarization of the electric field and the resulting vertical position of the charged nano-pigments. (b) Microscope image of microcapsules in a working prototype. Image adapted with permission from Ref. 20, used under a Creative Commons Attribution 2.0 Generic (CC BY 2.0) license. (c) A photograph of the Amazon Kindle e-reader tablet adapted with permission from Ref. 21, used under a Creative Commons Attribution 2.0 Generic (CC BY 2.0) license.

applied,[25] resulting in the microcapsules being arranged in a closely packed monolayer. This arrangement facilitates a thinner overall packaging of the microcapsules. In addition, it was found that adding an oil-soluble high molecular weight polymer to the electrophoretic fluid increased image stability to 12 days and, importantly, without increasing the fluid viscosity.[26] In the initial stage of electrophoretic display developments, a "flash reset" was necessary prior to rendering a new image. This process involved resetting the positions of all particles to a uniform, known state, allowing for a more predictable and reliable transition to the desired grayscale level in the subsequent image. Using an algorithm[27] that stores the history of each pixel's switching for a certain amount of time allows for addressing 16 levels of grayscale without flashing. Parasitic polarization in the microcapsule polymeric binding material leads to a dwell time dependence:[28] the impulse required to switch a pixel to a new optical state depends on the time that the pixel has spent in its previous optical states. This issue has been greatly researched and resolved through careful selection of the materials used.[29,30]

4.2.2 *Color system*

Color displays for dual particle systems have been achieved through the addition of a color filter array (CFA), as visualized in Fig. 6(a), or multi-particle systems, as visualized in Fig. 6(b).

Different methods have been explored to create CFA; these include direct printing[35] or photolithography[36] of a color resist and laminated CFA films.[37] However, CFAs, such as RGB or RGBW, use area sharing, in which each full-color pixel consists of three or four sub-pixels, respectively. This method limits the display area for each color, leading to suboptimal brightness

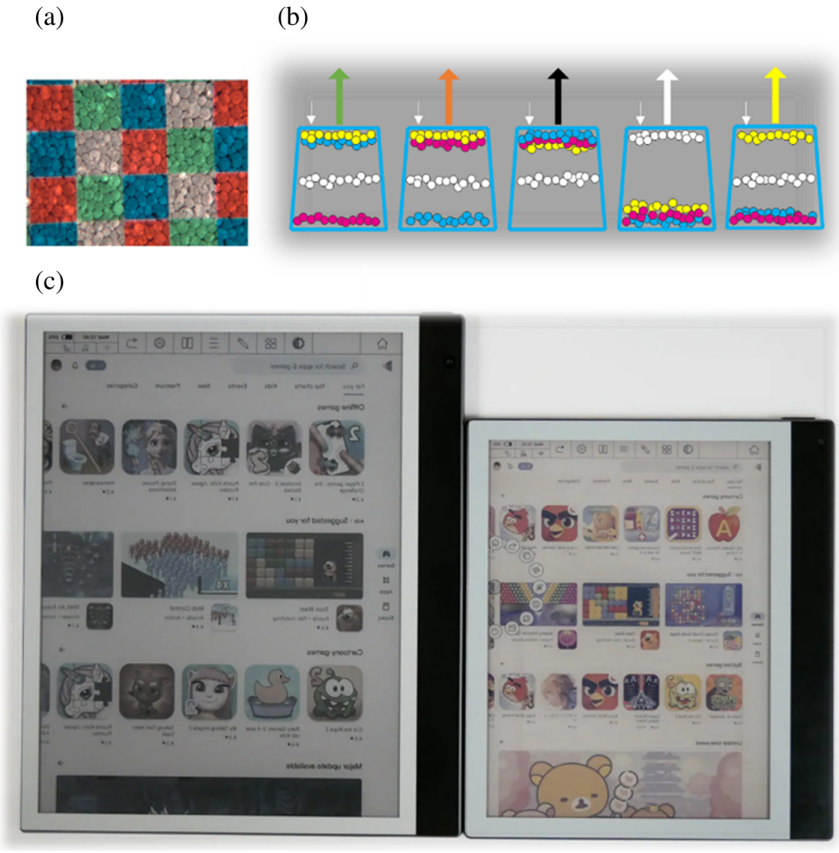

Fig. 6 Color electrophoretic reflective display technology, based on (a) superimposed color-filter arrays. Adapted with permission from Ref. 31, copyright (2006), Society for Information Display. (b) A multi-color particle system.[32] (c) CFA based device "Inknote Color Plus" on the left and "Bigme Galy" device on the right with a multi-particle system offering brighter colors.[33] The image is taken at the same location and same illumination, showcasing the increased brightness of multiparticle systems. Image adapted with permission from Ref. 34, copyright (2023), Good e-reader.

levels. Furthermore, the implementation of a color filter to divide monochromatic pixels into three colored pixels inevitably leads to a reduction in the overall resolution.

To overcome these limitations in filter-based color electrophoretic displays, current research is exploring multi-particle systems. The key concept behind multi-particle systems is to make use of different electrophoretic mobilities as well as charge polarity and intensity to separate the particles.[38] Using waveforms, these particles are pushed and pulled to mix colors and produce specific shades. The EInk Spectra system uses black, white, and colored particles (either red or yellow). For full-color displays, EInk's Advanced Color ePaper (AceP) combines white with cyan, magenta, and yellow particles, enabling it to render up to 50,000 colors,[32] akin to newspaper prints. Figure 6(c) compares two commercial displays using CFA (left) and a multi-particle system (right) under the same illumination condition. The brightness difference is clearly perceived.

4.3 Improving Switching Speed of Microencapsulated Electrophoretic Display Device

Various studies have been carried out to improve the response time. One approach is to use low viscosity[39] to increase electrophoretic mobility; however, this deteriorates bistability. Other approaches focus on improving the driving waveforms[40] or on picture drawing algorithms based on the content.[41] Yet another suggestion is to use the inverse electrorheological (IER) effect,[42] essentially reducing the viscosity briefly during the switching time. It was found that such an IER effect can be induced by the rotation of LC molecules,[43] briefly leading to some carrying hydrodynamic motion. Adding LC molecules leads to a 2.8 times reduction of response time while cutting the applied voltage in half.

4.4 Total Internal Reflectance Electrophoretic Displays

TIR displays use TIR for bright images and "frustrated" TIR for dark ones, achieving high contrast and fast visual changes. In TIR, light in one medium reflects internally when hitting a lower-index medium at a steep angle. Frustrated TIR happens when a third, higher-index medium is close to the interface, letting some light pass or be absorbed. This technology was first reported in 1997.[44]

4.4.1 *Working principle*

For TIR electrophoretic displays, the switching mechanism is achieved through the movement of charged particles in and out of the evanescent field.[45] To optimize the angular response, TIR displays are constructed using hemispheres.[46] Charged electrophoretic absorbing particles are hosted inside a liquid below the reflective hemisphere array. As depicted in Fig. 7(a), absorbing particles are pulled out or into the evanescent field, allowing the light to be reflected or absorbed, respectively.

The phenomenon of TIR occurs when light is incident upon an interface from a high refractive index material n_1 to a low refractive index n_2 at an angle of incidence θ that exceeds the critical angle θ_c given as

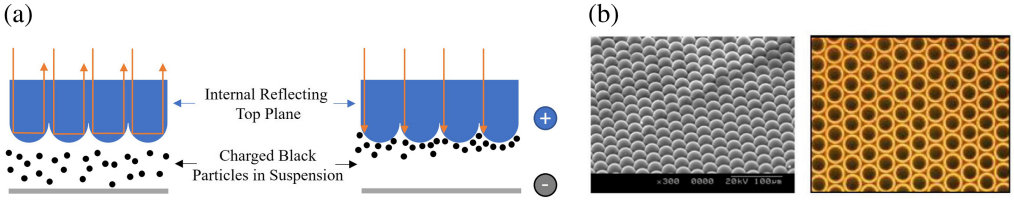

Fig. 7 TIR electrophoretic display concept. (a) Schematic representation[43] of the working principle, showing TIR reflection and frustrated TIR when the polarity of the applied electric field draws the absorptive charged black particles into the evanescence wave field. (b) SEM image (left) of a fabricated reflection plane consisting of spheres in an index matching layer, as well as an optical microscope image showing the reflection rings and dark areas of normal incident light. Image adapted with permission from Ref. 173.

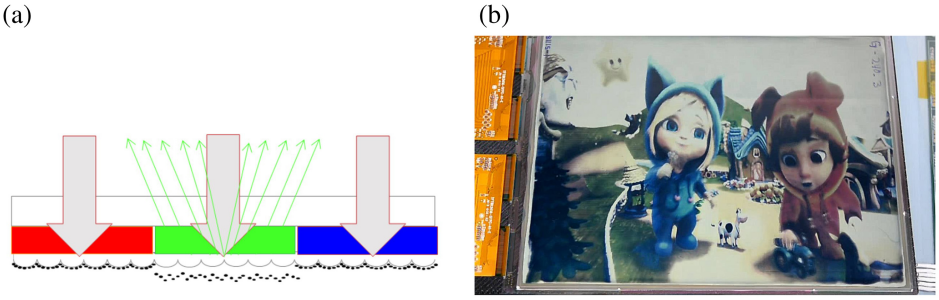

Fig. 8 TIR electrophoretic color display. (a) Schematic of TIR display with an RGB CFA; green is in the reflective state, and red and blue are in the absorptive state. (b) A picture of a tablet implementing this technology. Adapted with permission from Ref. 48, copyright (2019), Wiley.

$$\theta_c = \arcsin\left(\frac{n_2}{n_1}\right). \tag{4}$$

For angles of incidence less than the critical angle, light is transmitted through the interface. Conversely, for angles of incidence greater than the critical angle, the light undergoes TIR and is reflected back into the first medium. As depicted in Fig. 7(b), upon normal incidence light, these hemispheres exhibit a bright reflective ring until the light's angle of incidence surpasses the critical angle, causing the hemisphere's center to reflect less light. For normal incidence, the reflection is given as

$$R = 1 - \left(\frac{n_2}{n_1}\right)^2. \tag{5}$$

In practice, the said hemispheres are formed from high refractive index nano-composite material $(n_1 \sim 1.9)$ and low-index adjacent medium, such as fluroniated hydrocarbon $(n_2 \sim 1.2)$; normal incidence reflections on the order of ~60% can then be expected.

The size of the hemispheres can be made as small as 2 μm in diameter. This reduces the device thickness and thus the required travel distance for the absorbing nanoparticles, yielding a higher switching time and reducing energy consumption, as well as easing the material constraints with respect to material attenuation coefficient. Color displays are achieved incorporating CFA on top of the microsphere array, as depicted in Fig. 8.

CLEARink released a number of working prototypes, for example, at SID 2019[48] a 9.7″ diagonal eTIR display demonstrating video and color capabilities including grayscale [see Fig. 8(b)], showcasing a very small power consumption of merely 0.029 mJ/cm^2.

4.5 Outlook

The main challenge of microcapsule electrophoretic displays is the switching speed. The response time is usually as long as hundreds of milliseconds.[49] This limits the application to static or slow-moving images. Current challenges for TIR electrophoretic are mostly related to commercial scalability, as well as improving the color gamut, increasing video speeds, reducing ghosting, and improving the general reliability of device. A potential long-term issue for TIR-based reflective displays is that they cannot operate in transmission by design. Thus, this makes a stacked CMY(K) pixel design difficult and ultimately limits the potential for achieving high color saturation/brightness.

5 Liquid Crystal

Backlight LCDs make up most of commercially available emissive displays, while presenting one of the first reflective display technologies. LCDs were first suggested for display applications in 1968 at the International Liquid Crystal Conference in Ohio. The prototype presented by George Heilmeier of RCA[1] generated substantial interest and triggered the start of LCD developments for many industrial companies. The next crucial step toward a robust, "television-ready"

LCD was the invention of the twisted nematic display (TN-display) by Martin Schadt and Wolfgang Helfrich in 1970.[50] The TN principle and technologies derived from it remain one of the central foundations of most LCDs to this day. However, one of the challenges has been their continuous power consumption required to maintain an image. This led to the exploration of more power-efficient display technologies. A significant breakthrough came in 1994, when Yang et al.[51] demonstrated that dispersing a polymer in cholesteric liquid crystals (ChLCD) or using a cell with inhomogeneous surface anchoring resulted in long-term bistability. This bistable property enables the LC molecules to maintain their original orientation for a long time even after the electric field is removed, greatly reducing power consumption for static images. Both TN and cholesteric LCD technologies are presented in the following sections.

5.1 Twisted-Nematic Liquid Crystal Displays

5.1.1 *Working principle*

The TN-cell[52] is the most basic LCD technology; it consists of an LC sandwiched between two crossed polarizers and a reflective layer on the backside. The first polarizer in this setup polarizes incoming light in one direction. When turned off, the LC rotates the polarization of the traversing light by 90 deg, allowing it to pass through the second polarizer and be reflected on the backside mirror. When the LC is turned on, the incoming light's polarization is no longer rotated and is blocked on the second polarizer [see Fig. 9(a)].

Polarizer-based LC technology can attain a maximum reflectivity of 50% because a polarizer filters out half of the unpolarized ambient light.

5.1.2 *Implementation*

TN-cell based reflective LCD is not bistable by nature. Memory-in-pixel (MIP) technology is often employed to reduce power consumption.[53] MIP designates the technology of integrating static random-access memory circuits into every pixel unit, effectively holding the voltage until a pixel state needs to change. To further reduce energy consumption, it is suggested to only refresh the rows and lines of the display that need to display movement.[54] As MIP LCDs are fully digital displays compared with conventional analogue active-matrix LCD, attaining grayscale values is more challenging. In terms of optical characteristics, light diffusion methods must be included in a reflective LCD to avoid a mirror-like look. Such diffusion can either be achieved through the addition of scattering back electrodes or top diffuser films.

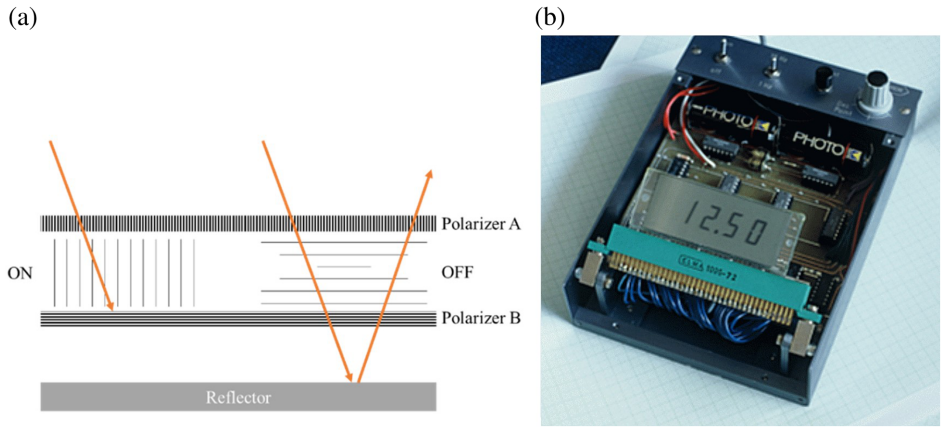

Fig. 9 Reflective TN display: (a) schematic representation: unpolarized light first passes through polarizer A, where it is linearly polarized. In the OFF-state, the liquid crystal rotates this polarization by 90 deg, enabling it to pass through polarizer B and reflect off the back-reflector. In the ON-state, polarization is not rotated; hence it is blocked by polarizer B. (b) Early TN LCD prototype 1972. Adapted with permission from Ref. 47 under a Creative Commons Attribution-Share Alike 3.0 license.

5.1.3 *Outlook*

TN-cell based reflective LCD has an economic advantage over other technologies as they can directly leverage the decades of emissive LCD display manufacturing. MIP displays allow for the reduction of power consumption significantly, but they also limit the range of available colors and grayscale. This is due to the intrinsic limitations in the amount of memory at each pixel site (bit depth), which in turn determines the number of colors that can be displayed. Currently, 6-bit color MIP panels and 3-bit and 1-bit black-and-white panels are usually commercially available, restricting these displays to a smaller color palette (max. 64 here) and fewer grayscale levels. Finally, white state reflectivity is still limited to within 7% to 18% in commercial displays.[55]

5.2 Zenithal Bistable Display

Zenithal bistable displays (ZBDs), a pioneering advancement in the realm of LC display technology, derive their name from the term "zenith," indicative of the viewer's line of sight in relation to the display surface. This nomenclature is emblematic of the display's unique perspective, emphasizing an overhead or top-down viewing angle. The bistability is a key feature, enabling the display to hold an image with no power consumption until a change is required.

5.2.1 *Working principle*

The functional mechanism intricately controls the orientation of nematic LC molecules using a precisely patterned grating surface.[56] This grating, characterized by its distinct grooves, shapes the energy landscape, leading to the elastic deformation of the LCs and the formation of disclinations, or irregular alignment points, known as defects.[57] These disclinations stabilize the LC molecules in two distinct states: the defect (D) state, in which molecules are aligned at a low tilt, and the continuous (C) state, characterized by near-vertical alignment.[56] Central to the switching mechanism between these bistable states is the flexoelectric effect, a result of the significant elastic deformation around the grating grooves.[58,59] This effect generates polarization that responds to external electrical pulses, facilitating the controlled reorientation of the LC molecules between the D and C states. The ability of these states to remain stable without the need for continuous electrical input highlights the efficiency and low-energy design of ZBDs.[60] This sophisticated interplay of flexoelectric polarization and surface-induced molecular orientations is fundamental to the unique functionality of ZBDs.

5.2.2 *Implementation*

In ZBDs, the control over nematic LC molecules' orientations is achieved through the synergistic effects of a patterned grating surface and a non-altering rubbed polymer surface. The grating, by its design, induces the formation of local alignment states—either the D state, or the C state. These states are localized responses to the grating's microstructure. On a device level, the LC layer is sandwiched between one grating and a rubbed polymer surface. The molecule orientation on the polymer surface stays constant but can be switched at the grating. The resulting two bistable states are called the "hybrid aligned nematic" (HAN) state, denoting a state in which the molecules go through vertical to planar, and the TN state,[61] denoting a 90-deg twist between alignments, as visualized in Fig. 10(a). Furthermore, in general, the typical layers of a ZBD include front and rear polarizers, LC material, alignment layers, and electrodes.

5.2.3 *Outlook*

In general, ZBDs were among the first LCDs to exploit the flexoelectric effect, previously deemed too weak for practical applications, and they introduced nano-replication techniques into the LCD manufacturing process.[59] The initial commercial application of ZBD technology manifested in electronic point-of-purchase (ePOP™) signage within the retail sector[60] (see 10b). It has been demonstrated that ZBD technology facilitates latching at voltages below 20 V and achieves switching speeds exceeding 80 microseconds per line,[62] enabling the update of an entire e-book page in as little as 10 milliseconds. However, the reflectivity of ZBDs in their white state, approximately 30%—primarily due to the front polarizer—renders this technology less

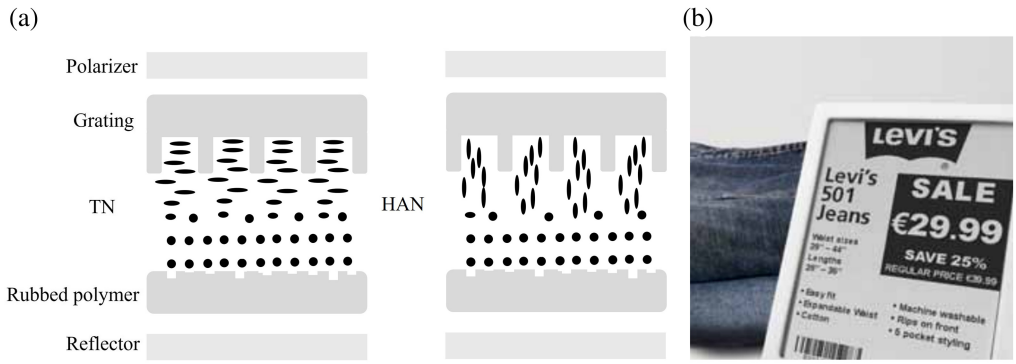

Fig. 10 The Zenithal Bistable Display. (a) A schematic depiction of the basic structure consisting of a front polarizer, grating, liquid crystal (LC) layer, rubbed polymer, and reflector. An electric potential causes the LC layer to switch between a TN state and a HAN state, both of which are bistable. (b) Photograph illustrating a typical use case of ZBDs as a shelf label, specifically the ZBD EPOP 900 model. (Datasheet, copyright 2011 ZBD Displays Ltd.).

appealing for e-paper applications compared with the approximate 50-60% white state reflectivity of conventional newspapers.

5.3 Cholesteric Liquid Crystal Displays

The terminology "cholesteric" was first introduced in the scientific community by Georges Friedel in 1922,[63] recognizing the initial identification of this particular state of matter within cholesterol esters by Friedrich Reinitzer in 1888.[64] Subsequent to this initial discovery, instances of cholesteric liquid-crystalline states have been reported in a variety of substances that bear no inherent connection to cholesterol.

5.3.1 *Working principle*

Cholesteric refers to a phase of LC in which the molecules are arranged in layers with a helical stacking pattern. For normal incidence, the reflected wavelength is given as[65,66]

$$\lambda_0 = n_a p \cos(\theta), \tag{6}$$

where n_a is the average refractive index, p is the helical pitch, and θ is the angle between the helical axis and the direction of propagation.

As can be seen from Eq. (6), reflectivity is concentrated around a specific central wavelength. Consequently, wavelengths deviating from these central peaks contribute less to the total reflectivity, leading to an overall decrease. The bandwidth of the cholesteric reflection is given as

$$\Delta\lambda = \Delta n p, \tag{7}$$

where $\Delta\lambda$ is the birefringence of the LC and p is the pitch. The LC molecules have an inherent electric dipole moment. By applying an electric field, these molecules experience a torque, causing the LC molecules to align along the field direction. This alignment alters the pitch p, thus tuning the reflected wavelength λ_0. The key advantage of cholesteric LC displays is their bistability, with two textures at zero electric field: the reflective planar and the non-reflective focal conic. Here, 'texture' refers to the macroscopic molecular arrangement, as shown in Fig. 11(a).

Upon normal incidence, a cholesteric LC surface reflects the component of the light that is circularly polarized in the same handedness as the CLC, transmitting the other component, and thus it cannot reflect more than 50% of unpolarized light.[70] At oblique incidence, the reflected or transmitted light becomes elliptically polarized.

The brightness can be significantly increased using a stack of two cells with opposing helical twists. Each cell reflects light with a specific handedness of circular polarization. The first cell lets through light of one handedness, which is then reflected by the second cell, enhancing the display's brightness. Defects in the cholesteric crystal structure lead to scattering and non-ideal

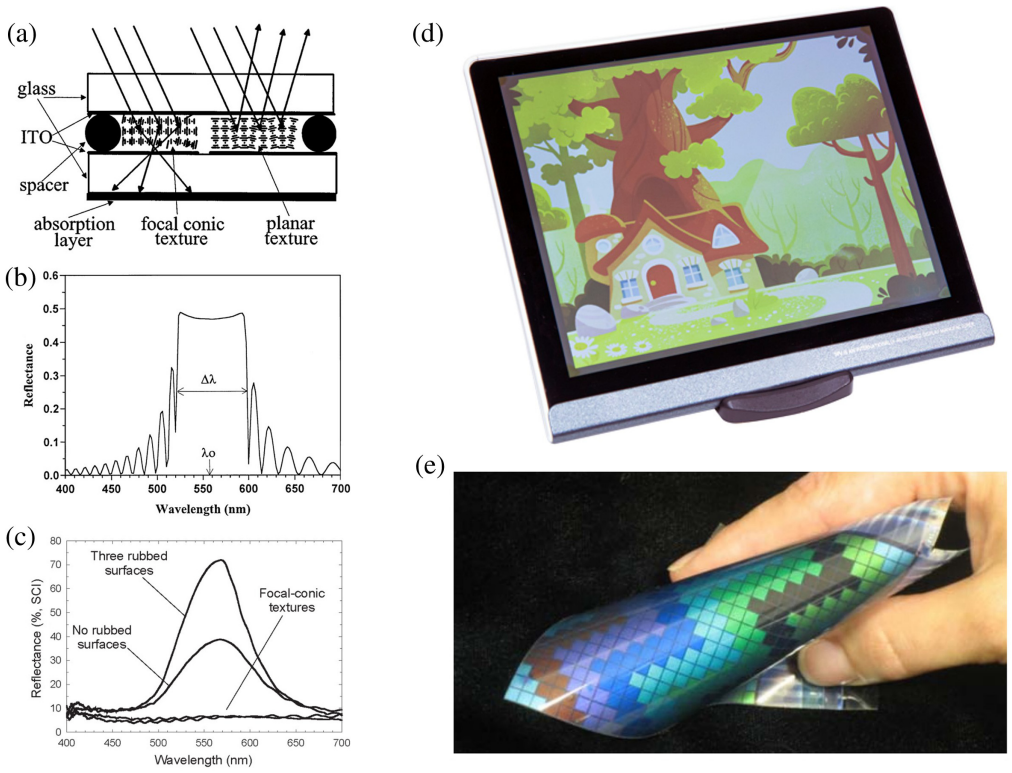

Fig. 11 Bistable cholesteric reflective display design and examples. (a) The schematic design of a bistable cholesteric reflective display,[67] illustrating the layered composition and functional elements. (b) Exemplary reflection spectrum of said cell showing the reflection bandwidth $\Delta\lambda$ and central wavelength λ_0[67] and (c) two-layer stacked cell with and without surface treatment (rubbing) to improve reflection. (d) 7.5-inch full-color ChLCD display. Image adapted with permission from Ref. 68, copyright (2023), AUO. (e) A flexible cholesteric display, demonstrating the technology's adaptability and potential for diverse applications. Image adapted with permission from Ref. 69, copyright (2008), radtech.

reflection conditions. This can be improved using rubbed contact-surfaces. "Rubbed" refers to surfaces that have been mechanically treated by rubbing them in a specific direction to align LC molecules. This rubbing process induces an alignment of the LC molecules along the direction of the rubbing, which helps to minimize defects in the cholesteric structure. As a result, this treatment has been shown to yield an increase in reflectivity of up to 70%[71] [see Fig. 11(c)].

5.3.2 *Implementations*

A single pixel [Fig. 11(a)] in a cholesteric reflective display is made up of a cross-section of multiple layers, each of which contributes distinct capabilities to the pixel's overall functioning. The topmost layer is a glass substrate that provides the pixel with physical structure and protection. Directly behind this is a layer of indium tin oxide (ITO), which acts as a transparent, conductive layer, allowing electric fields to be applied across the pixel. The pixel's core layer is made of cholesteric LCs. This layer's properties change in reaction to applied electric fields, allowing it to selectively reflect light with a specified circular polarization, or "handedness" and transition between various states, resulting in the display's brilliant and dark appearances.

A spacer separates the cholesteric LC layer from the bottom ITO layer. This spacer guarantees proper layer alignment and separation, which is crucial for preserving the LC's orientation and operation because, upon exerting shear stress on a cholesteric film, such as through substrate pressing, the system readily transitions back to the slightly more energetically stable planar texture.[72] The bottom ITO layer performs the same function as the top ITO layer, completing the pair of electrodes required to alter the state of the cholesteric LC layer. An absorption layer is often put directly beneath this, typically with black paint. When the LC is in the focused conic

state, this layer absorbs forward diffracted and scattered light, improving the pixel's contrast and overall display performance. For display applications, the image needs to be temperature invariant. Because most cholesteric materials are temperature dependent,[73,74] much research has been dedicated to solving this issue, such as using dopants that show opposite changes in helical twisting behavior with temperature to effectively cancel each other's influence.[75] Another important technological challenge is the peak wavelength on the incident angle, as can be seen from Eq. (6). This dependence can be eased by integrating a diffuser film[76] and thus broadening the distribution of reflection angles, albeit at the expense of peak reflectivity. Recently, AU Optronics Corporation (AUO) started to roll-out reflective colorful ChLCD displays, as shown in Fig. 11(d). Figure 11(e) shows a flexible prototype by Kent Displays.

5.3.3 *Outlook*

Reflecting and bistable cholesteric LC displays have been commercially accessible. These devices have evolved with features such as increased luminosity, multi-color output via stacked layers, and high-contrast monochrome display from a single layer. Their current limitation is the switching speed, which usually lies on the order of a second,[77] limiting the potential applications in mobile devices.

6 Micro-Electro-Mechanical Systems

MEMS-based systems enable rapid, reversible, and often low-power geometric reconfiguration. These trademarks make them well suited for reflective display technologies. Digital micro-mirror devices (DMD) have shown wide adoption in projection systems through the commercialization of micro-mirror arrays that pivot to modulate light.[78] Pixtronix's digital micro-shutter technology is an experimental emissive direct-view display that uses laterally translating shutters for light modulation.[79] By eliminating inefficient optical components, the Pixtronix MEMS-based shutters achieve over 50% optical transmission efficiency and reduced power consumption compared with LCDs. However, the technology has seen limited commercial adoption. MEMS-based direct view displays have not yet hit a wider market despite significant research efforts, most notably by Qualcomm with their "Mirasol" project, an interferometric modulators (IMOD) display, originally introduced by Mark Miles in 1997.[80] Despite Mirasol not achieving the expected commercial success, MEMS-based direct-view displays continue to intrigue.

6.1 Interferometric Modulator Display

Each sub-pixel of an IMOD consists of a Fabry–Perot etalon composed of a movable metallic mirror and a semitransparent glass upper layer [see Fig. 12(a)]. When light falls on the glass, it is split into two beams, with one beam reflected on the glass and one on the metallic surface. The traveled distance difference between the two beams results in a phase shift that affects the

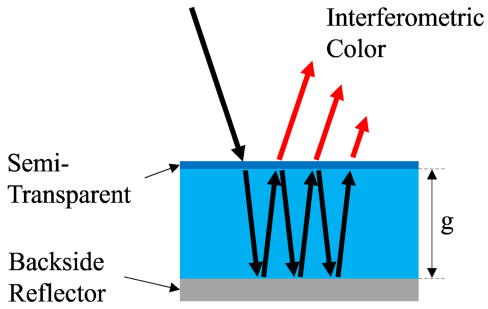

Fig. 12 Schematic drawing of the IMOD concept. Incoming light strikes a semi-transparent layer, where it is partially reflected and partially transmitted into a resonant cavity. Within this cavity, the light undergoes multiple reflections between the layers. Outgoing light of a specific wavelength then constructively interferes with the incoming light, leading to the color perception of that element. This process allows for precise control over the displayed color by tuning the gap g between the layers.

interference pattern of the reflected light. Tuning the gap between the glass and metallic layer changes the phase shift and thus the wavelength at which constructive interference occurs. This sets the perceived color of the individual sub-pixels.

For the most simplistic IMOD, which consists of a single layer with a reflective backplane, the gap (g) to enhance a specific wavelength λ is given as

$$g = m\frac{\lambda}{\cos(\theta)2n}, \tag{8}$$

where m is an integer $(1,2,3,\ldots)$, n is the refractive index of the medium between the layers, and θ is the angle of incidence. For normal incidence $\theta = 0$ and considering air $n = 1$ to be a medium, Eq. (8) simplifies to

$$g = m\frac{\lambda}{2}. \tag{9}$$

To create black, the gap g is reduced such that the reflected wavelength maxima is moved outside the visible spectrum and absorbed within a thin film within the stack. This is accomplished through electrostatic actuation, essentially collapsing the metal membrane onto the thin film stack. To avoid failure due to stiction in the collapsed state, stiction bumps are introduced.[81] In real devices, multiple layers might be used; in such cases, it is advised to refer to the transfer matrix method to compute the reflected color.

6.1.1 *Implementations*

Figure 13 shows the concept and full-scale realized tablet prototype of a Mirasol Qualcomm display. Each pixel can switch between a reflective colored state and an absorptive black state, in which the initial gap of the subpixel cavity controls the reflected wavelength.

As can be deduced from Eq. (8), IMODs possess by design an inherent property of incident-angle sensitivity, resulting in observable variations in perceived colors dependent upon the angle of incidence. To mitigate this issue, a diffuser can be introduced on top of the Imod pixel array,[83] as depicted in Fig. 14.

As mentioned in the previous section, the initial height of the Imod sub-pixel defines the reflected wavelength. However, as in all reflective display technologies, the use of a horizontal RGB leads to suboptimal contrast due to area sharing, which reduces the white state reflectivity. Thus, an innovative single-mirror continuously tunable pixel design that uses interferometric absorption,[85] instead of reflection was proposed. Single mirror interferometric (SMI) color regulation is achieved using interferometric absorption [see Fig. 15(a)]. Incoming light, interfering with reflected light, produces standing waves with varying peaks and nulls based on the light spectrum. By strategically placing a thin absorber at a null for a specific wavelength, selective non-absorption allows for reflection of that spectral component. All other wavelengths are absorbed, resulting in a saturated color reflection. Figure 15(a) displays the reflected color as a function of the absorber-mirror gap. In practice, the mirror is mobile, and the absorber is fixed on the substrate. This essentially allows each pixel to be modulated over the entire visible

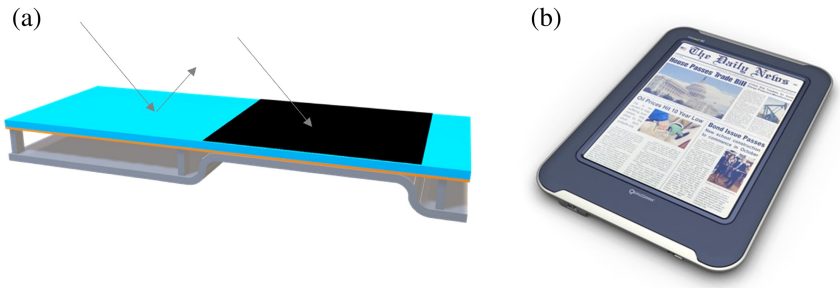

Fig. 13 The IMod architecture and full-sized display prototype. (a) Schematic drawing of a pixel element showing the on (color) and off (state);[82] (b) picture of a prototype tablet utilizing the Qualcomm Mirasol.

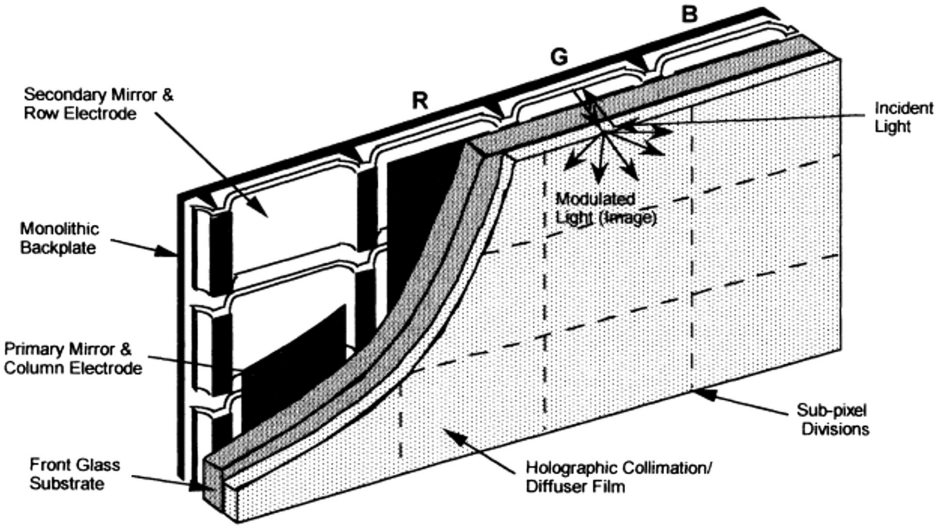

Fig. 14 Schematic view of a Qualcomm Mirasol display unit, including, in particular, a front-facing diffuser film to reduce angle dependence. Adapted with permission from from Ref. 84, copyright (1999), Society of Photo-Optical Instrumentation Engineers (SPIE).

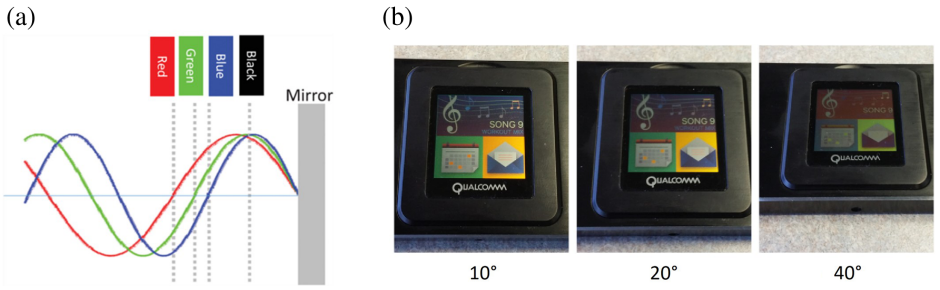

Fig. 15 Interferometric absorption-based continuous color tuning: (a) schematic illustrating the principle of color regulation through strategic placement of absorbers in standing light waves. (b) Off-axis viewing examples: camera directed at 10 deg off surface normal, 20 deg, and 40 deg. Image adapted with permission from Ref. 86, copyright (2015), Optica.

spectrum, drastically increasing the reflectivity. On the other hand, SMI also suffered from angle dependence. Figure 15 shows an SMI display at different angles of incidence. One can perceive the color shift in Fig. 15(b), when observing from 10 deg or 40 deg.

In recent years, a graphene membrane-based IMOD (GIMOD) was proposed;[87] it potentially allowed for refresh speeds of up to 400 Hz and 5 μm pixel resolution, which translates roughly into a smartphone with a 12K display resolution, a 20 times increase in resolution compared with the typical phone resolution (QHD, 2560×1440 pixels). Current designs of GIMOD are fabricated using graphene-covered micro-holes, essentially creating a voltage-controlled graphene micro-drum, where the initial cavity and the subsequent deflection of the drum control the reflected wavelength. This allows for analog control over the pixel's color, yielding continuous full-spectrum reflective-type pixels. Simulations show a CR of 1:3 utilizing 29 layers of graphene. For vibrant reflective displays, this number must be increased by at least three times. Nevertheless, the high frame rate, resolution, and full-spectrum pixel are promising avenues.

6.1.2 *Outlook*

MEMS-based IMOD reflective displays have been developed[88] into fully functional prototypes with impressive optical characteristics, such as 80% white state reflectivity, CRs reaching 1:30,[86] and fast switching times of 120 Hz,[85] which allows for full video playback. As with any movable

structure in the microscale, hermetic sealing and packaging become very important for the longevity of the device. Gas-impermeability of graphene might ease the packaging constraints for GIMOD devices; however, their CR of 1:3 needs to be improved.

6.2 Other MEMS-Based Reflective Display Technologies

Hereafter, two further early-stage MEMS-based potential reflective display technologies are briefly introduced. Both approaches still need substantial developments to move from early-stage demonstrators to large-scale production.

6.2.1 *Mechanical light shutter*

A mechanical light shutter functions by actively introducing an object into and out of the light's trajectory, casting a shadow on an absorptive or reflective layer. Such implementations can be observed in Jutzi et al. work.[89,90] Figure 16 demonstrates the utilization of micro-flaps to alternate between a reflective state (flaps raised, producing a white pixel) and an absorptive state (flaps lowered, resulting in a black pixel). To optimize the CR, the anchoring system of the flaps should take as little visible area as possible; thus a good balance between flap size and anchor needs to be found. Increasing the size of the flaps comes with drawbacks such as slower switching speeds, reduced pixel density, and potentially compromised reliability. Nevertheless, this design offers the possibility of excellent CRs.

6.2.2 *Mechanically tunable metasurface reflectivity modulator*

Recently, an MEMS-based actively tunable metasurface was shown to be able to modulate the reflectivity in the visible spectrum.[91] The working principles and a microscope image of a segmented display prototype are shown in Fig. 17. The idea is to vertically displace a membrane punctuated with a regular pattern of holes, each hosting a stationary nano-disk, which effectively tunes the surface geometry and subsequently, light absorption and reflectivity.

7 Electrowetting

Electrowetting is the act of applying an electric potential to modulate surface wettability. This phenomenon has found numerous applications in microfluidic devices[92] and varioptical lenses.[93] In 2002, Robert Hayes and Bokke Feenstra from Philips Research filed a patent[94] and published[95] their results one year later, in which they demonstrated a video speed response time optical switch to be utilized in display systems, highlighting the potential of such systems. As with many reflective display innovations, the main motivation was to propose a video-capable solution. The key idea behind electrowetting-based reflective displays is colorant transport in and out of a light path by expanding and retracting colored liquids within a pixel unit. Similar to the Mirasol display, substantial research efforts by Philip's spinoff Liquidvista, later owned by Amazon and then Samsung, never fully substantiated into a commercial product.

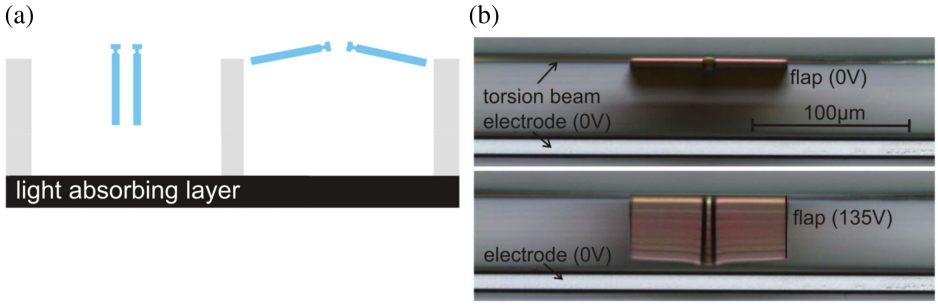

Fig. 16 Micro-mechanical light shutter. (a) Schematic of the actuation method and (b) optical microscope image of the final prototype device.[90] The applied voltage was 135 V. Images adapted with permission from Ref. 89, copyright (2010), SPIE Proceedings.

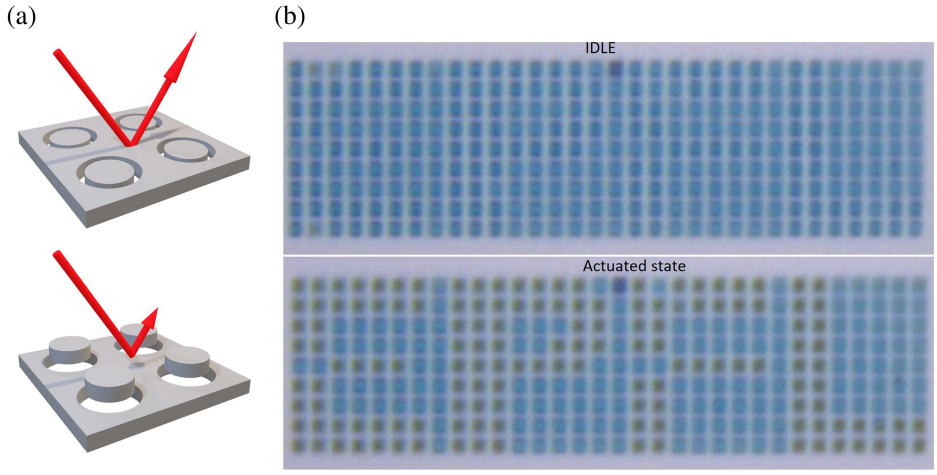

Fig. 17 Mechanically tunable metasurface reflectivity modulator. (a) Schematic drawing of working principle, aligned surfaces reflect light, whereas displaced surfaces absorb it. (b) An optical microscope image shows the EPFL logo on a segmented display, visible when switched from idle to actuated states. Image under open access CC-BY 4.0. from Ref. 91, copyright (2023), ACS Photonics.

7.1 Working Principle

The Young–Lippmann's equation[96] captures the electrowetting phenomenon in its most basic form. It describes how the contact angle of a conductive liquid changes in response to an applied voltage between a liquid and an isolated substrate, given as

$$\cos(\theta) = \cos(\theta_0) + \frac{CV^2}{2\gamma}, \tag{10}$$

where θ is the contact angle after applying the voltage, V, θ_0 is the initial contact angle, and C is the capacitance between the liquid and substrate, which depends on the insulation material $(\frac{\epsilon_0 \epsilon_r}{d})$. Finally, γ is the interfacial tension.

In most electrowetting-based pixels, two fluids coexist. The first is usually an insulating oil ink. The second is a conductive transparent liquid electrolyte, such as DI water. At equilibrium, the colored oil film lays between a hydrophobic insulator coating of an electrode. With the application of a potential, the stack becomes no longer energetically favorable, resulting in the water displacing the oil while reducing its contact angle from θ_0 to θ with respect to the hydrophobic layer, as can be seen in Fig. 18(a). The colored oil film can essentially be opened and closed like a curtain.

The oil displacement happens in different stages,[98] namely oil film rupture (initiation stage), oil-dewetting, and finally a slower oil drop rearrangement stage. A threshold voltage is needed for the initial oil rupture. Charges accumulate at the interface between oil and water when electricity is applied, creating pressure and causing the oil to undulate due to Rayleigh-Taylor

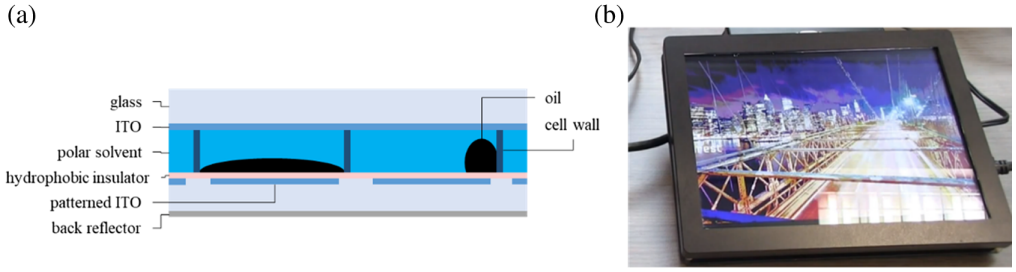

Fig. 18 Electrowetting display mechanism: (a) schematic of a unit pixel cell demonstrating the transition between expanded and contracted oil states, indicative of the "curtain-like" movement of the colored oil film modulated by potential application; (b) Actual device implementation showcasing the technology in practice. Image source from Ref. 97. Video: The Electrowetting Display IEEE Spectrum YouTube channel.

instability.[99] As these undulations increase, the water ultimately breaks through to the dielectric substrate, resulting in a three-phase contact line. Due to the induced change in contact angle by electrowetting, the water then forces the oil to one side. The reverse mechanism or receding process is more straightforward, with the oil re-wetting the hydrophobic surface as the water retracts.

7.2 Implementations

Electrowetting-driven reflective pixels pose several challenges that need to be addressed for reliable operations and increased optical performance. For instance, the contrast between covered and uncovered states, often referred to as "white area fraction" or "aperture," needs to be maximized. Naturally, the colored oil cannot completely disappear from the light path. In the retracted state, there will still be some fraction of the pixel that will display the colors of the oil. This fraction depends on the pixel size and oil film thickness. Figure 19(a) depicts the relation between the pixel size and aperture for different oil thicknesses. The fraction is computed by assuming a hemispherical sphere oil droplet in the contracted state hosted in a rectangular pixel. Using volume conservation between expanded and contracted oil, the surface fractions can be easily computed.

One can observe that, for pixel sizes below 40 μm and 5 μm oil thickness, the aperture drops below 50%. Thus, to increase the display resolution, thinner oil thicknesses are needed. To minimize light bleeding through, oils with higher molar extinction coefficients are thus more desirable.

Another challenge to overcome is contact angle hysteresis (CAH). CAH is a well-known physical phenomenon in electrowetting. It is defined as the difference between the advancing contact angle and the receding contact angle observed at the same voltage. Figure 19(b) illustrates an example in which there is an aperture discrepancy, albeit with the same final applied potential. Increasing the voltage from 0 to 20 V yields a smaller aperture than decreasing the voltage from 30 V to 20 V. CHA makes it more challenging to control precise gray levels in electrowetting displays. CHA has been attributed to random pinning forces, which are caused by surface heterogeneities at smaller scales.[88] These forces can be successfully reduced utilizing an increasing alternating voltage scheme,[101] which leads to sufficient vibrational energy to overcome the pinning forces.

Finally, it is also important to account for the so-called "backflow problem." In electrowetting systems, a dielectric material is used to separate the conducting electrodes from the liquid. When applying a potential to the system, charge trapping can occur in the dielectric layer. These remaining charges can cause the fluid to flow back, even when a constant DC voltage is applied. Charge trapping significantly impacts the stability of electrowetting-based devices. Asymmetric alternative polarity driving schemes[102] are said to reduce charge trapping. In essence, any

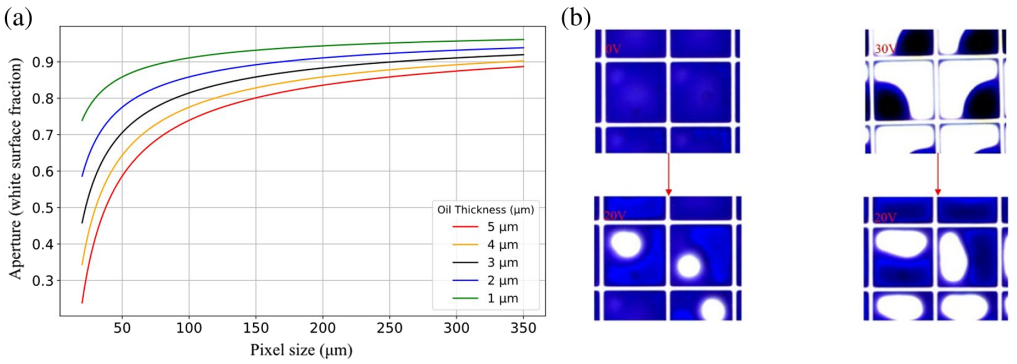

Fig. 19 Electrowetting challenges. (a) Relationship between pixel size and aperture across different oil film thicknesses. In smaller pixels, thicker films decrease the visible white/transparent area. However, thinner films let more light through, which can lower the contrast. (b) Optical microscope images showing contact angle hysteresis.[100] Adapted with permission from Ref. 100 under CC BY 4.0 DEED, copyright (2021), Frontiers in Physics.

remaining trapped ions are removed by applying a reset pulse, a small voltage drop with opposite polarity at the signal termination point.

7.3 Outlook

Electrowetting-based displays have undergone excessive research and development both in the commercial industry as well as in academic research. Despite their potential for color and video reflective display technology, this innovation never ventured beyond proof-of-concept prototypes. Manufacturing difficulties, such as proper sealing and longevity under varying conditions, might have been the cause. Moreover, with advancements in display technology, particularly in terms of resolution, electrowetting displays have become less competitive in terms of image quality because oil thickness and pixel size are tightly linked. Nevertheless, electrowetting technology remains a promising area of research with potential applications in areas such as e-readers, smart glasses, and flexible displays. Current efforts are focused on low-power sunlight-readable electronic billboards as this application is less stringent on display resolution.

8 Electrochromic

Electrochromism refers to the phenomenon in which a material's optical properties – transmittance, absorbance, or reflectance—can be reversibly and semi-persistently modified under the application of an electrochemical potential difference. The word "electrochromisn" was first introduced in 1961 by Platt[103] upon his findings that the absorption and emission spectrum of certain dyes could be shifted by applying an electric field. Eight years later, the use of electrochromic materials for display applications was suggested by Deb.[104] By then, the slow switching speed was noted as a potential challenge. To this day, electrochromism has been utilized in various applications that do not require fast switching, most notably in smart windows, first reported by Granqvist and Carl M. Lampert Kim in 1984,[105,106] as well as auto-dimming rear-view mirrors.[107,108] Further applications are protective eyewear[109,110] and adaptive camouflage.[111,112]

8.1 Working Principle

The core principle of electrochromic materials is their ability to change their absorption bandgap, by adding or removing electrons through redox reaction. Electrochromic materials can most often be switched between a transparent ("bleached") state and a colored state or between two colored states. Polychromic materials may exhibit several colors.[113,114] The primary mechanisms to achieve a change in electron state are redox reactions, either directly induced or through ion intercalation. The specifics depend on the type of electrochromic material.

8.2 Implementations

Electrochromic materials can generally be classified according to their solubility,[115] leading to different device architectures, as depicted in Fig. 20.

Type I EC materials remain soluble in both their reduced and oxidized states. Examples include viologen and heptyl. In device architectures, these materials often have their electrochromic species dissolved directly within an electrolyte, which is sandwiched between two

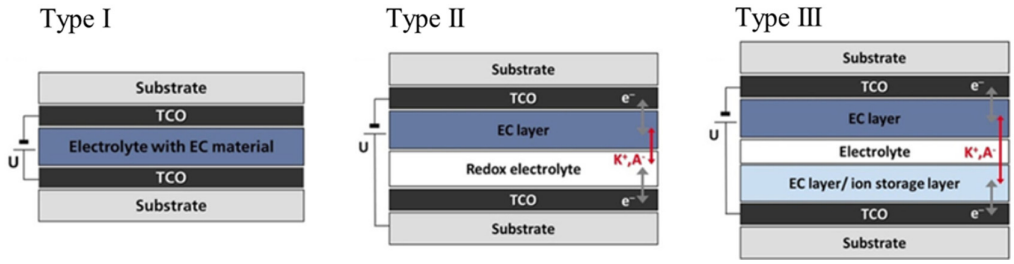

Fig. 20 Electrochromic display. (a) Schematic diagrams of three types of electrochromic devices are shown: (a) type I, which operates in a solution-phase; (b) type II, a hybrid system; and (c) type III, also known as the "battery-like" ECD. K^+ represents cations, which could be Li^+ or H^+, and A^- represents anions, for instance, ClO_4^-, Cl^-, BF_4^-, or PF_6^-. Images adapted with permission from Ref. 115 under CC BY 4.0 DEED, copyright (2020), Chemistry Europe.

transparent conductive oxide substrates. Although the fabrication of such devices is relatively straightforward, a critical challenge arises in ensuring the sealing of the devices to avert potential electrolyte leakage. Furthermore, there is an inherent requirement for a continuous supply of current or voltage to uphold their redox states, which could lead to increased energy consumption.

Type II EC materials remain soluble when in their colorless redox state but transition to form a solid film upon the electrode surface when subjected to specific conditions. Devices leveraging Type II materials integrate a redox mediator in the electrolyte, acting as a counterbalance during the redox reactions. This interaction, although promising, does have its challenges. A significant one is the "loss current," a consequence of the direct contact between the redox electrolyte and the EC layer. However, innovations, such as electronic barrier layers[116] and catalytic IrO_x layers,[117] provide potential solutions to this challenge.

Type III EC materials stand apart due to their inherent solidity in both redox states. This means that they consistently form an insoluble film on the electrode surface. The gamut of Type III materials is extensive, comprising groups IV and V transition metal oxides, conductive polymers, Prussian blue, and certain metal polymers. In device configurations, these materials typically feature in thin-film "battery-like" setups. Such a device incorporates two substrates coated with transparent conductors, an electrochromic layer, and another layer designated for ion storage or as an additional electrochromic layer. The addition of an ion-storage layer with ample charge capacity ensures a complete and effective color transition, resulting in a device that boasts impressive electrochemical stability.

In practical applications, particularly when considering reflective displays, Type III often emerges as the preferred choice due to its inherent stability and enhanced optical properties.

Electrochromic materials transition from a neutral to an "excited" state during redox reactions, challenging the development of bistable electrochromic devices (ECDs) as they tend to revert to their stable, lower-energy states. This reversion diminishes the longevity of the desired optical state. To counter this, proton-coupled electron transfer[118] and bond-coupled electron transfer[119] have been implemented. These methods avoid the formation of high-energy intermediates, which can destabilize the material, reducing its effective life and performance. Electrode materials are fundamental in electron transfer processes. They require meticulously designed energy levels (Fermi levels) that synchronize with those of electrochromic materials. Proper alignment ensures efficient electron transfer and minimizes reverse transfers.[120] Metal dendrites, irregular tree-like structures, can form on electrode surfaces. Their presence disrupts the uniformity of the electron transfer, leading to inconsistent color transitions. To combat this, copper ions have been integrated into bismuth-based systems. The copper ions oxidize bismuth atoms, creating a smoother, spherical morphology. This morphology reduces the chance of dendrite growth, ensuring a consistent electron transfer and uniform color change.[121] For enhanced device responsiveness, multivalent ions, such as Al^{3+}, are incorporated into tungsten oxide WO_x materials. These ions facilitate rapid and reversible ion insertion/extraction.[122] The increased electrostatic forces between ions lead to an accelerated electron transfer, improving the device response time. To diversify the color palette and fasten switching, electrochromic materials are paired with metasurfaces, including Fabry–Perot cavities[123,124] and metallic nanoslits.[125] These metasurfaces induce structural colors and optimize charge-diffusion characteristics. The result is a broader color spectrum and reduced switching times.

Innovative pixel designs utilizing both lateral and vertical configurations have emerged.[126,127] Examples include Urano et al.'s three-layered CMY ECD[128] and RICOH's full-color, flexible matrix display (see Fig. 21). These leverage vertically stacked electrochromatic elements. Such stacking allows for brighter color displays, and their flexibility enhances the device adaptability.[129]

8.3 Outlook

EC displays offer numerous benefits: they are inexpensive, low-power, insensitive to viewing angle, and capable of semi-bistability. Although electrochromism has already been commercially successful in smart window and glare-reduction applications, commercial displays are still limited to simple monochromatic segmented displays. Continued research and development in electrochromic materials and device architectures are essential to unlocking their full potential and

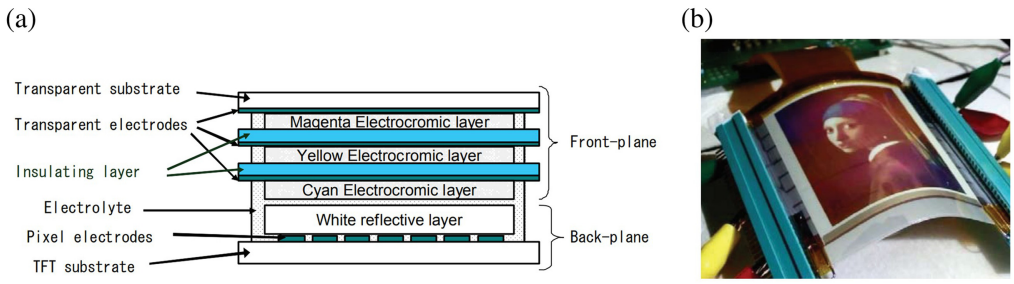

Fig. 21 Multi-layered full-color reflective electrochromic pixel. (a) Schematic representation of a unit and (b) a photograph depicting a full-color, flexible, active-matrix-based implementation of the display design. Images adapted with permission from Ref. 129 (permission pending), copyright (2013), Ricoh.

drive advancements, particularly concerning switching speed, which currently lies around 0.8 Hz.[77] Innovations, such as the introduction of PEDOT nanotube arrays, have shown promise in achieving ultrafast switching speeds compatible with moving-image display technology, suggesting that continued innovation in material science could overcome existing limitations in switching speeds and pave the way for more versatile electrochromic displays.[130]

9 Phase Change

Phase-change materials exhibit reversible transitions between amorphous and crystalline phases in response to an external stimulus, such as heat, light, or electrical current. Concurrently, variations in physicochemical attributes, encompassing alterations in optical absorbance, and electronic conductance, are observed.[131] The phases can be switched very fast, typically 300 ns for GeTe,[132] 50 ns for $Ge_2Sb_2Te_5$, 40 ns for $GeSb_2Te_4$, and 30 ns for GeSb4Te_7.[133] Thus, phase-change materials (particularly the germanium antimony tellurium alloy $Ge_2Sb_2Te_5$) have been greatly used in information storage devices since the 1960s,[134] for instance, in optically re-writable DVDs (DVD-RAMs)[135] and non-volatile resistive based electronic memories.[136] Hosseini et al.[136] pioneered the idea of utilizing nanometer-thin phase-change materials and transparent conductors to generate color-switchable reflective pixels based on an incident angle-insensitive strong IMOD.[137] Due to their solid-state nature based on phase change materials, this type of display technology has been introduced as solid-state reflective display (SRD). However, due to limitations with electrical addressing, discussed in the following section, the previously mentioned switching times cannot be obtained with current display designs. Nevertheless, the fact that this technology does not require any moving parts makes it especially interesting from a manufacturing point of view as devices could be made using conventional standard vacuum sputtering, bypassing the requirement for sophisticated encapsulation.

9.1 Working Principle

The material science behind phase change is complex. It has been shown that the switching from crystalline to amorphous states when directly applying current occurs due to rapid heat-induced dislocation nucleation, electrical wind force transport, and eventual jamming in the crystal, which leads to amorphization.[138] By contrast, the amorphous-to-crystalline transition occurs by heating the material above its crystallization temperature. Upon cooling down, the atoms reorganize into a crystalline lattice, resulting in a lower resistance state. The variations in optical properties arising from these structural modifications can be further understood by examining the corresponding changes in bonding strengths. It was found that the crystalline phase exhibits resonant bonding, whereas the amorphous phase shows covalent bonding.[138] The greater degree of electron delocalization in resonant bonding materials, as opposed to covalent bonding, can have a significant impact on the optical characteristics of the material. The higher level of interaction between delocalized electrons and incident electromagnetic waves produces specific absorption, transmission, and reflection characteristics, resulting in optical performances that differ significantly from materials having localized covalent bonding. On a broader scale, individual phase-change based pixel designs differ. However, the primary objective is to engineer

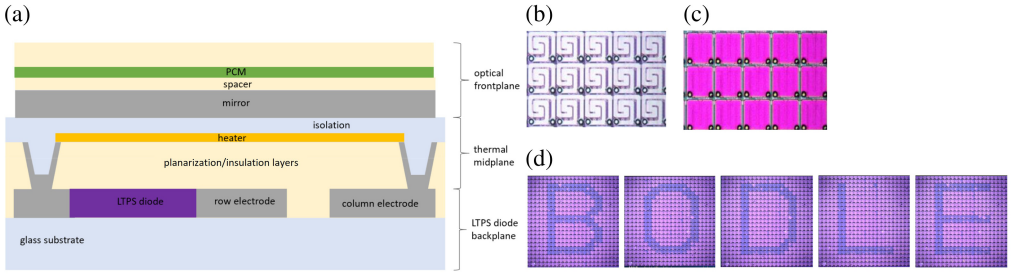

Fig. 22 Microheater-based phase change display system (Fig. 21). (a) Schematic of the SRD pixel structure (b) microheater array, (c) the assembly comprising a mirror and thin-film interference stack, and (d) a microscope photograph demonstrating a 24×24 pixel region being dynamically updated with a sequence of letter. Images adapted with permission from Ref. 140 (permission pending), copyright (2019), Society for Information Display.

a wavelength-dependent tunable resonance that is then tuned by the phase-change material, inherently altering the resonance conditions due to a change of optical properties when switching from an amorphous to a crystalline state.

9.2 Implementations

When directly applying current to the switch state, the material undergoes a partial phase change until a low-resistance pathway is established.[139] This pathway subsequently functions as a channel for the residual current, impeding a full-phase transition. This phenomenon is referred to as the "filamentary switching issue."[139] Utilizing nanoscale pixels can effectively reduce this issue. However, addressing such a vast number of pixels individually and simultaneously presents a challenge. As the number of pixels in a display grows, the amount of computing power and energy needed by the circuits that control each pixel also rises significantly.[140] Thus, alternative more homogenous switching methods need to be envisioned. To avoid the filamentary switching issue, much effort has been devoted to the design of decoupled micro-heaters as a means to uniformly fully switch the phase-change material,[140] as shown in Fig. 22. A typical phase-change-based pixel structure is depicted in Fig. 22(a). The SRD pixel consists of three primary layers: an electronic substrate directing drive signals to specific pixels, a microheater that converts electrical signals to uniform thermal pulses, and finally an optical layer reflecting specific colors in stable phase-change material states via strong interference effects.

9.3 Outlook

Efforts to increase color saturation can be achieved by a higher refractive index and lower loss materials than GST or GeTe, such as antimox trisulphide (Sb_2S_3) and antimony triselenide (Sb_2Se_3).[141] Although noticeable switchable color changes are possible, little has been demonstrated of producing a black state, which is needed for a fully functional display. When switching phases, the real part of the refractive index GST material usually exhibits a change of roughly 1.5 to 2, whereas the absorption coefficient can be altered by more than 3.[142] Essentially, for a given pixel design, the resonance sensitivity to a variation in optical constants needs to be increased for a black state to exist. In such a state, the resonance would need to be shifted outside the visible domain. So far this remains a challenge. Furthermore, the use of microheaters severely limits the switching times. Frequencies of mere 2 Hz are reported.[140] With approximately 100 mJ/cm^2[142] microheaters also consume more energy per frame than electrostatic-driven systems.

10 Tunable Photonic Crystal

The theoretical work of Yablonovitch[143] and John[144] serves as the foundation for the idea of photonic crystal materials. Materials can be created to alter photon properties in a manner comparable to how conventional semiconductor crystals alter electron properties. The propagation of light waves through the substance can be controlled by periodically structuring the material. This makes it possible to produce photonic band gaps, which are wavelength bands that cannot pass through the substance. Since its early days, photonic crystals have been successfully applied in

various examples, such as filters, sensors, solar cells, and recently smart windows to regulate building energy consumption.[145] Photonic crystals have emerged as an interesting technology for reflective displays due to their continuous color tunability, essentially avoiding the need for sub-pixelation for display colors. This can lead to higher color purity and increased resolution.

10.1 Working Principle

1D photonic crystals' colorful appearances result from interference and reflection. The wavelength that is coherently scattered is centered on λ and is estimated by the Bragg-Snell equation:[146]

$$\lambda = 2D\left(n_{\text{eff}}^2 - \cos^2(\theta)\right)^{\frac{1}{2}}, \tag{11}$$

where λ is the wavelength of the reflected light, n_{eff} is the average refractive index of the photonic materials, D is the diffractive plane spacing, and θ is the Bragg angle of incidence.

Based on Eq. (11), the different ways to alter the reflected wavelength can be inferred, namely by modifying three variables: the diffractive plane spacing, the average refractive index, or the Bragg incidence angle.

10.2 Implementations

Most photonic crystal-based reflective pixels are based on acting on the inter-plane distance to modulate the reflected wavelength. The key challenges are to find fast-switching methods as well as ways to respond to the inherent angle incidence dependence of such photonic crystals, which can be seen in Eq. (11).

For the most part, inter-plane distance variations are achieved in electrochemical swelling-driven color change displays[147] and electrokinetic-driven reflective displays.[148] Although crystalline structures have shown excellent color tunability, their practical application has been severely impeded by their intrinsic angle dependency. It has been demonstrated[149,150] that colloidal structures that are made up of particles with sizes similar to optical wavelengths and exhibit short-range order but lack lattice periodicity, exhibit independence of the incident angle. These systems[148,151] have therefore been seen as promising candidates for color-tunable reflective displays, albeit with lower peak reflectivity values of generally around 25% to 30% [see Fig. 23(c)].

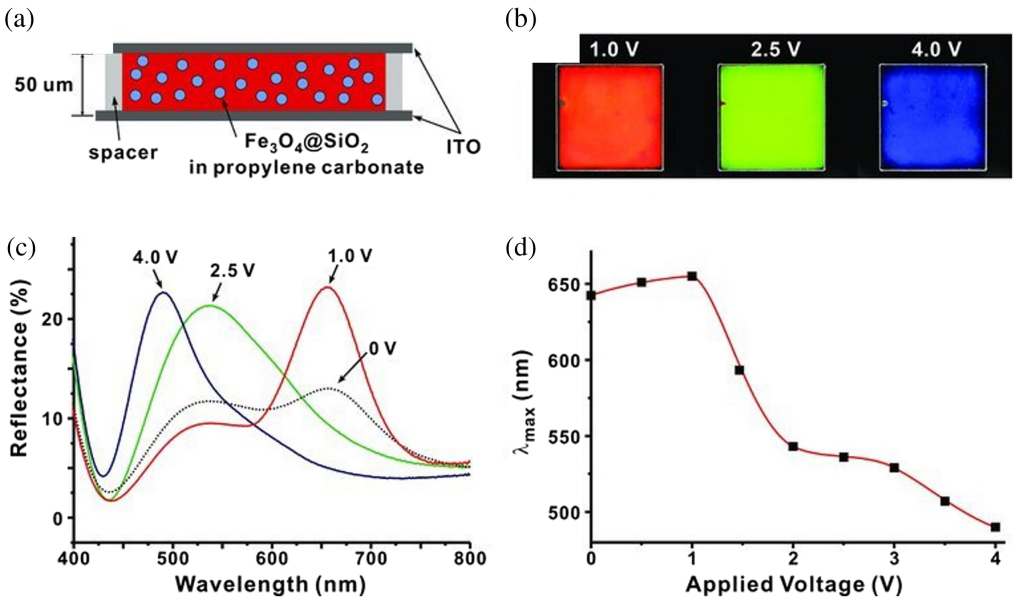

Fig. 23 Photonic display pixel. (a) Schematic design of the photonic display pixel. (b) Photographs at varying bias voltages: 1.0 V, 2.5 V, and 4.0 V. (c) Reflection spectra recorded at increasing bias voltage levels. (d) The 165 nm shift of the photonic band position from 655 to 490 nm, governed by the applied voltage. Images adapted with permission from Ref. 148, copyright (2010), Advanced Materials.

10.3 Outlook

Switching times of approximately 50 ms[148] have been documented in tunable photonic crystals, which, although not yet suitable for video applications, demonstrate potential for improvement. One possible approach to enhancing the switching speed is through the employment of lower-viscosity liquids, which may facilitate a faster response time. Furthermore, the trade-off between angle independence and color intensity presents another challenge. Although amorphous photonic structures have shown reduced angle independence, they also exhibit reduced peak reflectivity and less vibrant colors. This is due to the incoherent scattering events caused by their disordered arrangement, resulting in weaker constructive interference and diminished color intensity. Hierarchical photonic structures[152,153] have been proposed to produce both angle-independent and bright colors, but further investigations and optimization are required to address these limitations and fully realize the potential of tunable photonic crystals in display technologies. Finally, it is worth mentioning that, although continuous color can be produced, producing white without resorting back to an area-sharing subpixel layout, such as RGB, has yet to be shown. Commercially, two companies are pioneering modulation approaches using photonic crystals. Opalux focuses on color-tunable Photonic Ink, and Nanobrick works on full-spectrum tuning using SiO_x-coated nanoparticles.

11 Discussion

A comparative performance map is depicted in Fig. 24, and used hereafter for the discussion. Microcapsule electrophoretic displays, featuring reflectance up to 44%,[154] CRs of 23,[155] and a frequency of 2.1 Hz,[156] have achieved commercial success. They offer an optimal blend of readability and energy efficiency with a refresh energy density of 0.58 mJ/cm^2.[157] The modulation of TIR using electrophoretic mechanisms further enhances these displays, achieving reflectance up to 83%,[158] maintaining a contrast of 20,[158] and reaching frequencies of around 30 Hz,[48] while maintaining an impressively low refresh energy density of 0.029 mJ/cm^2.[48]

ChLCDs, utilizing cholesteric LCs, present reflectance around 35%,[77] and CRs close to 10.[159] Their limited response time of 0.8 Hz,[77] however, restricts their utility in mobile devices, reserving them for specific applications, such as shelf-labels, in which high refresh rates are not essential. Similarly, electrochromic displays, offering reflectance between 40%[160] and 47%[161] and contrasts up to 12,[160] operate at a frequency of approximately 1 Hz;[160] thus they too face challenges for integration into mainstream mobile devices.

Electrowetting displays, although nascent, exhibit promising metrics with reflectance peaking at 65%,[162] though they have a modest contrast of 1.7.[162] Their highlight is a frequency that reaches 62 Hz,[162] indicating a potential for fluid video playback.

Phase change displays, characterized by their non-volatile solid-state pixels, present a reflectance of 44%,[142] comparable to commercial electrophoretic displays. Despite this notable similarity in reflectance, other metrics such as a contrast of 2.5,[142] a frequency of 2 Hz,[142] and a high refresh energy density of 104 mJ/cm^2[142] underline areas that need improvement for this technology to achieve a competitive standing. Additionally, producing a black state by the sole use of SRD pixels has not yet been demonstrated.

Tunable photonic crystals stand out for their potential to display continuous colors within individual pixels. Their current implementations, achieving white state reflections between 30% and 60%[151] and reported 20 Hz frequency,[5] could be an interesting venue to explore further. The switching speed needs to be improved to yield video playback possibilities, as well as further reduction of the angle dependence and the ability to show white.

Concluding, MEMS-based reflective displays, especially the interferometric absorption-based design by Qualcomm, are exemplary. They manifest a 90% reflectance,[86] a contrast of 30,[84] and an impressive frequency of 120 Hz,[86] complemented by a PPI of 363[86] and a minimal refresh energy density of 0.004 mJ/cm^2.[86]

In evaluating the appropriateness of display technologies for various application sectors, it is imperative to first consider the key performance metrics that are critical for each sector. This approach ensures a more targeted and effective application of emerging display technologies. In the following, we assess the suitability of the reflective display technologies discussed in this review for selected applications.

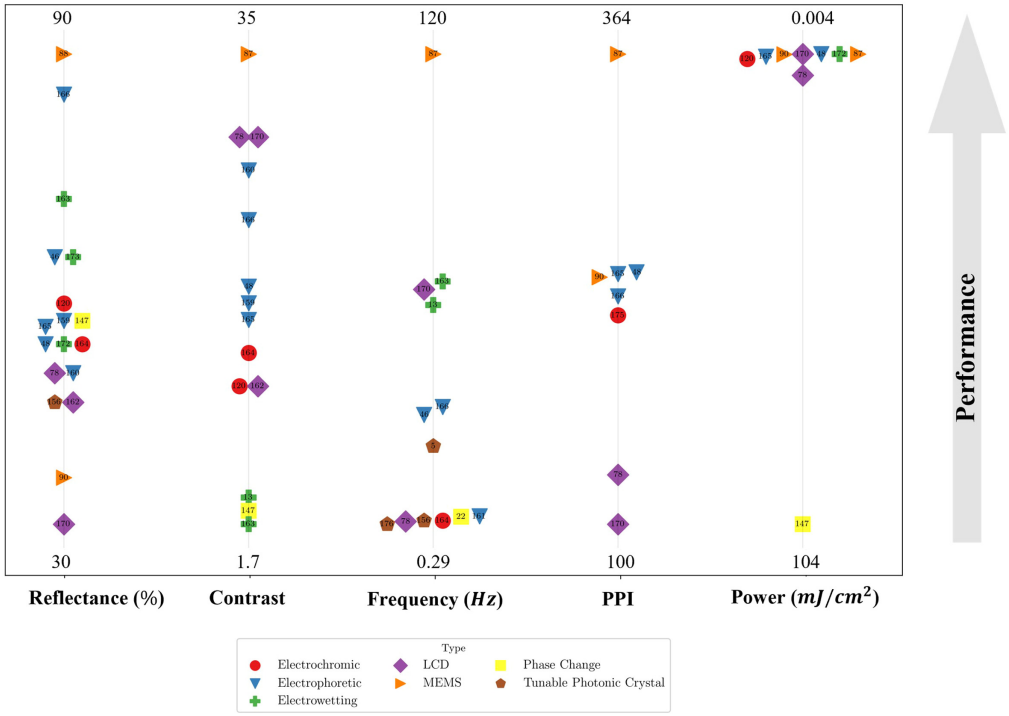

Fig. 24 Performance map for reflective display technologies: this representation compares diverse reflective display technologies based on their essential performance parameters. Microcapsule electrophoretic displays (reflectance: 44%,[154] contrast: 23,[155] and frequency: 2.1 Hz[156]) and their ChLCD (reflectance: 35%,[77] contrast: 10,[159] and frequency: 0.8 Hz[77]) and electrochromic counterparts (reflectance: 47%,[112] contrast: 12, frequency: 1 Hz[162]) find their niche in applications demanding static images given their constrained refresh rates. Conversely, emerging electrowetting displays, exhibiting up to 65% reflectance and a remarkable 62 Hz frequency,[155] signal promise for dynamic video renditions. Phase change displays, with a reflectance mirroring that of electrophoretic at 44%,[160] however, are marked by a considerable refresh energy density of 104 mJ/cm^2.[160] Albeit discontinued commercially, MEMS-based Qualcomm designs achieve a stellar 90% reflectance,[81] contrast-ratio of 1:30,[84] and a swift 120 Hz,[84] while being impressively efficient at 0.004 mJ/cm^2.[84] Numeric values can be found in Appendix A, Table 2.

11.1 Signage

Signage applications prioritize low power consumption, long-term image stability, and moderate refresh rates. ChLCDs are particularly well suited for this domain, offering image maintenance without continuous power and a modest reflectance of around 35%. Phase change displays, still in the emerging phase, also show promise for static signage due to their low power requirements and non-volatile nature, although their current slower switching speeds make them less ideal for dynamic content.

11.2 E-Readers

In the e-book and e-reader sector, key considerations include medium refresh rates, optional color, and high energy efficiency. Microcapsule electrophoretic displays, commonly known as E Ink, stand out in this category. They balance high readability, with reflectance up to 44%, and energy efficiency, with a refresh energy density of 0.58 mJ/cm^2, making them a preferred choice for devices used extensively over long periods.

11.3 Smartwatches and Mobiles

For smartwatches and mobile applications, in which high refresh rates, superior pixel density, and full-color capabilities are paramount, MEMS-based reflective displays take the lead. These emerging technologies boast superior performance metrics, including high reflectance

(up to 90%), impressive contrast (with a ratio of 30:1), and high-frequency operation (up to 120 Hz), making them increasingly relevant. With a pixel density of 363 PPI, these displays are especially suitable for devices that demand high-resolution visuals, ranging from advanced e-writers to premium consumer electronics. Smartwatches emerge as an especially ideal candidate for MEMS-based reflective displays due to their small display footprint (facilitating the packaging) and essential need for low-power operation as well as outdoor visibility.

11.4 Billboards and Large-Format Displays

For billboards and large-format displays, the focus is on sunlight readability and less stringent resolution requirements. Here, electrowetting displays, an emerging technology, presents a viable option. They offer low power consumption and effective sunlight readability, making them suitable for large-scale outdoor displays such as electronic billboards, for which high resolution is not the primary concern.

Beyond core metrics, the mitigation of inadvertent internal reflections is paramount in e-paper technology. Although these displays capitalize on ambient light reflection, undesirable internal reflections—often from thin-film interfaces—can compromise performance. Advanced techniques, such as index matching and multilayer destructive interference, have been employed to counteract these challenges. Notably, antireflective coatings inspired by nocturnal moth corneal patterns[163] have achieved reductions in spurious reflectivity to a mere 0.1% within the visible spectrum.[164] Raut et al. provided a thorough discussion on this reflection management.[165]

12 Conclusion

This review has covered a variety of reflective display technologies. Despite significant research efforts, reflective displays are generally absent in typical mobile devices such as smartphones and smartwatches. This is particularly critical given the inherent benefits of these displays, such as longer battery life and improved visibility in bright outdoor environments. The primary obstacles hindering their widespread integration into mobile devices are the current limitation of refresh speed and the compromised color vibrancy that many of these technologies exhibit. For example, although reflective LCDs are capable of video playback, their white state reflectivity is constrained to approximately 9%,[166] thereby affecting the saturation of displayed colors. By contrast, microcapsule electrophoretic displays showcase a considerably higher reflectance, reaching up to 44%,[165] but suffer from restricted refresh capabilities.

Within the realm of emerging technologies, ClearInk's TIR display technology offers a promising avenue for augmenting the update speed of electrophoretic-based displays. Concurrently, MEMS-based technologies are gaining prominence due to their inherent rapid switching times, high CRs, and relative energy efficiency. Recent developments in this field are particularly encouraging. For instance, preliminary research into tunable metasurfaces has revealed potential pathways for achieving broadband tunability in the visible spectrum with displacements of a mere 150 nm.[91] Furthermore, graphene-based IMODs have demonstrated remarkable capabilities, achieving refresh rates of up to 400 Hz and ultra-high resolution.[87]

The landscape of reflective display technologies, diverse and evolving, stands out for its unique advantages in the broader spectrum of display technologies. Quantum dot light emitting diode (QLED),[167] renowned for delivering impressive visuals in emissive displays, sets a high standard with its vibrant color reproduction and deep CRs. This technology excels in providing dynamic visual experiences, making it a top choice in settings for which image quality is paramount. By contrast, reflective displays carve their own niche. Their strength lies in their energy efficiency and superior visibility under bright ambient light conditions, aspects for which emissive displays such as QLED are less effective. Reflective technology, therefore, emerges as a practical alternative in environments where power consumption and outdoor readability are critical considerations. As ongoing research and development in reflective display technologies progress, the prospect of integrating these energy-efficient, high-performance display systems into conventional mobile devices is becoming increasingly feasible. The line between a static printed medium and a dynamic digital display could become remarkably indistinct.

13. Appendix A: Data for Comparison Graph

The refresh energy density is usually not directly given in the references cited but is computed from given power consumption, active area, and frame refresh time. Because some technologies are more experimental, not all data is available.

Table 2 Comparative study of performance metrics of reflective display technologies.

Type	Reflectance (%)	Contrast	Frequency (Hz)	Dots per inch (DPI)	Refresh energy density (mJ/cm^2)
Electrophoretic microcapsule	35[155] 44[154] 43[157]	23[155] 15[154] 14[157]	2.1[156]	226[157]	0.58[157]
Electrophoretic total internal reflection	55[46] 83[158] 40[48]	20[158] 16[48]	28[46] 30[158]	212[158] 227[48]	0.029[48]
LCD reflective	9[166]	25[166]	60[166]	69[166]	0.03[166]
LCD cholesteric	30[159] 35[77]	10[159] 25[77]	0.8[77]	100[77]	4.7[77]
Electrowetting	40[168] 65[162] 55[169]	1.7[162] 3.3[13]	62[162] 56[13]	N/A	0.013[168]
MEMS interferometric modulator	17[88]	80%[88]	40 Hz[170]	224[88]	0.05[88]
MEMS continuous color reflective	90[86]	30[85]	120[85]	364[85]	0.004[85]
Phase change	44[142]	2.5[142]	2[22]	N/A	104[142]
Electrochromic	40[160] 47[161]	12[160] 10[161]	1[160]	200[171]	1.1[161]
Tunable photonic crystals	60-30[151]	N/A	1[151] 0.125[172] 20[5]	N/A	N/A

Disclosures

The authors declare that they have no relevant financial interests in this manuscript and no other potential conflicts of interest to disclose.

Code and Data Availability

All data are given in Table 2.

Acknowledgments

The authors acknowledge the financial support by InnoSuisse (Grant No. 44027.1 IP-ENG).

References

1. H. Kawamoto, "The history of liquid-crystal displays," *Proc. IEEE* **90**(4), 460–500 (2002).
2. Y.-J. Huang et al., "Mini-LED, micro-LED and OLED displays: present status and future perspectives," *Light Sci. Appl.* **9**(1), 1–26 (2020).
3. S. Chen and S.-L. Lee, "Liquid crystal display and organic light-emitting diode display: present status and future perspectives," *Light Sci. Appl.* **6**(1), e17035 (2017).
4. Y. Shirasaki et al., "Emergence of colloidal quantum-dot light-emitting technologies," *Nat. Photonics* **7**(1), 13–23 (2013).
5. J. Heikenfeld et al., "Review paper: a critical review of the present and future prospects for electronic paper," *J. Soc. Inf. Disp.* **19**(2), 129 (2011).
6. B.-R. Yang, *E-paper Displays*, John Wiley & Sons (2022).
7. T. Goodman, *Overview of the Photometric Characterization of Visual Displays*, pp. 337–350, Springer International Publishing, Cham (2016).
8. Hertel, "Evaluating display reflections in reflective displays and beyond," *Inf. Disp.* **36**(2), 14–24 (2020).

9. DisplayMate, "Tablet and smartphone displays under bright ambient lighting shoot-out," (2023). (accessed 5 June 2023).
10. H. Chen, G. Tan, and S.-T. Wu, "Ambient contrast ratio of LCDs and OLED displays," *Opt. Express* **25**, 33643–33656 (2017).
11. R. Singh et al., "Improving the contrast ratio of OLED displays: an analysis of various techniques," *Opt. Mater.* **34**, 716–723 (2012).
12. M. Miles et al., "Digital paper™ for reflective displays," *J. Soc. Inf. Disp.* **11**, 209–215 (2003).
13. G. Yang et al., "Design, fabrication and measurement of full-color reflective electrowetting displays," *Micromachines* **13**, 2034 (2022).
14. M. E. Howard et al., "Gyricon electric paper," *J. Soc. Inf. Disp.* **6**(4), 215 (1998).
15. D. K. Deshmukh, J. Nirmalkar, and M. Haque, *Tb_3 Activated High-Color-Rendering Green Light Yttrium Oxyorthosilicates Phosphors for Display Device Application*, pp. 1–12, CRC Press (2020).
16. B. Comiskey et al., "An electrophoretic ink for all-printed reflective electronic displays," *Nature* **394**, 253–255 (1998).
17. R. J. Fleming, *Fast-Switching Mode with CLEARInk Structure*, Ch. 4, pp. 75–98, John Wiley Sons, Ltd. (2022).
18. H.-L. Kang et al., "Analysis of particle movement by dielectrophoretic force for reflective electronic display," *J. Disp. Technol.* **12**, 747–752 (2016).
19. T. Whitesides et al., "10.2: towards video-rate microencapsulated dual-particle electrophoretic displays," in *SID Symp. Digest of Tech. Pap.*, Wiley Online Library, Vol. **35**, pp. 133–135 (2004).
20. Wikipedia Contributors, "E ink — wikipedia, the free encyclopedia," (2023). https://en.wikipedia.org/w/index.php?title=E_Inkoldid=1157073256 (accessed 22 September 2023).
21. bfishadow, "Kindle voyage with origami cover," (2014). https://commons.wikimedia.org/wiki/File:Kindle_Voyage_with_cover.jpg (accessed 23 December 2023).
22. M. Wang et al., "Electrophoretic display device," US Patent 9,557,623 (2017).
23. H. Du, H. Gu, and X. Wang, "Silane-containing pigment particles for electrophoretic display," US Patent 9,382,427 (2012).
24. G. S. Roberts et al., "Electrostatic charging of nonpolar colloids by reverse micelles," *Langmuir* **24**, 6530–6541 (2008).
25. J. Albert et al., "Encapsulated electrophoretic displays having a monolayer of capsules and materials and methods for making the same," (2003).
26. R. M. Webber, "10.4: image stability in active-matrix microencapsulated electrophoretic displays," in *SID Symp. Digest of Tech. Pap.*, Vol. **33**, p. 126 (2002).
27. M. T. Johnson et al., "High-quality images on electrophoretic displays," *J. Soc. Inf. Disp.* **14**(2), 175 (2006).
28. T. A. Sjodin, "Methods for driving electro-optic displays," US Patent 8,289,250 (2017).
29. L. Cao et al., "Electrophoretic media with improved binder," US Patent Application 11/552,210 (2007).
30. R. J. Wilcox et al., "Electro-optic displays with reduced remnant voltage," US Patent 8,558,783 (2013).
31. A. Bouchard et al., "68.5l: Late-news paper: advances in active-matrix color displays using electrophoretic ink and color filters," in *SID Symp. Digest of Tech. Pap.*, Vol. 37, p. 1934 (2006).
32. E. Huitema and I. French, "E ink's technicolor moment: the road to color e-paper took two decades," *IEEE Spectrum* **59**, 30–35 (2022).
33. D. Hertel et al., "39-1: idistinguished paper:/i gamut rings of reflective ePaper displays with combined frontlight and ambient illumination," in *SID Symp. Digest of Tech. Pap.*, Vol. 53, pp. 485–488 (2022).
34. M. Kozlowski, "E INK gallery 3 vs e INK kaleido 3 color e-paper - good e-reader," https://goodereader.com/blog/e-paper/e-ink-gallery-3-vs-e-ink-kaleido-3?doing_wp_cron=1712047210.0039799213409423828125 (accessed 2 April 2024).
35. C.-M. Chang, C.-H. Chiu, and Y.-Z. Lee, "P-117: direct printed plastic color filter for color electrophoretic displays," in *SID Symp. Digest of Tech. Pap.*, Vol. 42, pp. 1545–1547 (2011).
36. Y.-H. Lai et al., "P-148l:ilate-news poster/i: direct photolithographic color filter for 14.1-inch flexible color electrophoretic displays," in *SID Symp. Digest of Tech. Pap.*, Vol. 43, pp. 1365–1367 (2012).
37. K. Akamatsu et al., "16.3: a 13-inch flexible color EPD driven by low-temperature a-si TFTs," in *SID Symp. Digest of Tech. Pap.*, Vol. 42, pp. 198–201 (2011).
38. H. Du and H. Zang, "Color display device," US Patent 9,285,649 (2016).
39. T. Hao, "Chapter 3 - The positive, negative, photo-ER, and electromagnetorheological (EMR)," *Stud. Interface Sci.* **22**, 83–113 (2005).
40. P. Bai, Z. Yi, and G. Zhou, "An improved driving scheme in an electrophoretic display," WO/2004/104977 (2004).
41. Z. Wang and Z. Liu, "The key technology of ereader based on electrophoretic display," in *2nd Int. Conf. Softw. Technol. and Eng.* (2010).
42. T. Hao, "Physics of electrorheological fluids," *Stud. Interface Sci.* **22**, 235–340 (2005).

43. Y.-D. Zhang et al., "Backflow effect enabling fast response and low driving voltage of electrophoretic e-ink dispersion by liquid crystal additives," *Sci. Rep.* **9**, 13981 (2019).
44. R. Laughlin and T. Hazelton, "Frustrated total internal reflection an alternative for optical cross-connect architectures," in *Conf. Proc. LEOS'98. 11th Annu. Meet. IEEE Lasers and Electro-Opt. Soc. 1998 Annu. Meet. (Cat. No.98CH36243)*, IEEE (1998).
45. M. A. Mossman, L. A. Whitehead, and S. P. Rao, "P-83: grey scale control of TIR using electrophoresis of sub-optical pigment particles," in *SID Symp. Digest of Tech. Pap.*, Vol. 33, p. 522 (2002).
46. M. A. Mossman, V. H. Kwong, and L. A. Whitehead, "A novel reflective image display using total internal reflection," *Displays* **25**, 215–221 (2004).
47. Wikimedia Commons contributors, "TN-LCD prototype image," https://commons.wikimedia.org/wiki/File:TN-LCD-schematic-MS-208kB.png (accessed 2 April 2024).
48. R. Fleming et al., "36-3: tablet-size eTIR display for low-power ePaper applications with color video capability," in *SID Symp. Digest of Tech. Pap.*, Vol. 50, pp. 505–508 (2019).
49. W. He et al., "Driving waveform design of electrophoretic display based on optimized particle activation for a rapid response speed," *Micromachines* **11**, 498 (2020).
50. W. D. Helfrich and M. D. Schadt, "Lichtsteuerzelle," 1793770A, filed (31 December 1972).
51. D.-K. Yang et al., "Control of reflectivity and bistability in displays using cholesteric liquid crystals," *J. Appl. Phys.* **76**, 1331–1333 (1994).
52. M. Schadt and W. Helfrich, "Voltage-dependent optical activity of a twisted nematic liquid crystal," *Appl. Phys. Lett.* **18**, 127–128 (1971).
53. Y. Nakajima et al., "22.4: invited paper: ultra-low-power LTPS TFT-LCD technology using a multi-bit pixel memory circuit," in *SID Symp. Digest of Tech. Pap.*, Vol. 37, p. 1185 (2006).
54. M. Tamaki et al., "A memory-in-pixel reflective-type LCD using newly designed system and pixel structure," *J. Soc. Inf. Disp.* **22**, 251–259 (2014).
55. S. K. Kaisha, "Thin-film electroluminescent panel," *Displays* **15**, 194 (1994).
56. A. Bezrukov and Y. Galyametdinov, "Orientation behavior of nematic liquid crystals at flow-wall interfaces in microfluidic channels," *Coatings* **13**(1), 169 (2023).
57. R. James et al., "Twist walls, disclinations and the in-plane switching structure," in *2nd Int. Workshop on Liquid Crystals for Photon (LCP-2008)*, pp. 66–67 (2008).
58. A. Buka and N. Éber, *Flexoelectricity in Liquid Crystals: Theory, Experiments and Applications*, World Scientific (2013).
59. J. Jones, "Defects, flexoelectricity and RF communications: the ZBD story," *Liq. Cryst.* **44**(12–13), 2133–2160 (2017).
60. J. Cliff Jones, "The zenithal bistable display: from concept to consumer," *J. Soc. Inf. Disp.* **16**(1), 143–154 (2016).
61. J. Chen, W. Cranton, and M. Fihn, *Handbook of Visual Display Technology*, Springer Publishing Company, Inc. (2011).
62. J. C. Jones et al., "26.3: low voltage zenithal bistable devices with wide operating windows," in *SID Symp. Digest of Tech. Pap.*, Wiley Online Library, Vol. 34, pp. 954–957 (2003).
63. G. Friedel, "Les états mésomorphes de la matière," *Ann. Phys.* **9**(18), 273–474 (1922).
64. H. Kelker, "History of liquid crystals," *Mol. Cryst. Liq. Cryst.* **21**, 1–48 (1973).
65. M. Mitov, "Cholesteric liquid crystals in living matter," *Soft Matter* **13**(23), 4176–4209 (2017).
66. M. Mitov, "Cholesteric liquid crystals with a broad light reflection band," *Adv. Mater.* **24**, 6260–6276 (2012).
67. D.-K. Yang, X.-Y. Huang, and Y.-M. Zhu, "Bistable cholesteric reflective displays: materials and drive schemes," *Annu. Rev. Mater. Sci.* **27**, 117–146 (1997).
68. AUO Corporation, "Eye care technologies at AUO," https://www.auo.com/en-global/technologies/index/Display/Eye_Care (accessed 2 April 2023).
69. T. Schneider et al., "UV cured flexible cholesteric liquid crystal displays," in *Radtech UV&EB Curing Technol., Tech. Conf. Proc.*, May, pp. 4–7 (2008).
70. P.-G. De Gennes and J. Prost, *The Physics of Liquid Crystals*, Vol. **83**, Oxford University Press (1993).
71. A. Khan et al., "27.4: super high brightness reflective cholesteric display," in *SID Symp. Digest of Tech. Pap.*, Vol. 32, p. 460 (2001).
72. D. Coates, "Cholesteric reflective displays," in *Handbook of Visual Display Technology*, pp. 2199–2222, Springer International Publishing (2016).
73. A. A. F. Froyen et al., "Electrothermal color tuning of cholesteric liquid crystals using interdigitated electrode patterns," *Adv. Electron. Mater.* **7**(2), 2000958 (2020).
74. Y. Huang et al., "Tuning the photonic band gap in cholesteric liquid crystals by temperature-dependent dopant solubility," *Opt. Express* **14**(3), 1236 (2006).
75. M. Schadt, "Liquid crystal materials and liquid crystal displays," *Annu. Rev. Mater. Sci.* **27**, 305–379 (1997).

76. T. Uchida and T. Ishinabe, "Reflective liquid-crystal displays," *MRS Bull.* **27**, 876–879 (2002).
77. VGA Cholesteric Display Modules and Controller Assemblies, Kent Display Incorporated, https://cdn.thomasnet.com/ccp/10069038/106600.pdf.
78. Y. Takashima and B. Hellman, "Review paper: imaging LiDAR by digital micromirror device," *Opt. Rev.* **27**, 400–408 (2020).
79. T. Brosnihan et al., "Pixtronix digital micro-shutter display technology: a mems display for low power mobile multimedia displays," *Proc. SPIE* **7594**, 759408 (2010).
80. M. W. Miles, "A new reflective FPD technology using interferometric modulation," *J. Soc. Inf. Disp.* **5**(4), 379 (1997).
81. M. W. Miles, "MEMS devices with stiction bumps," US Patent 7,554,711 (2009).
82. M. W. Miles, "5.3: Digital paper™: reflective displays using interferometric modulation," in *SID Symp. Digest of Tech. Pap.*, Vol. 31, pp. 32–35 (2000).
83. M. Kothari, "Method and device for compensating for color shift as a function of angle of view," US Patent 7,630,123 (2009).
84. M. W. Miles, "MEMS-based interferometric modulator for display applications," *Proc. SPIE* **3876**, 20–28 (1999).
85. E. K. Chan et al., "Continuous color reflective display fabricated in integrated MEMS-and-TFT-on-glass process," *J. Microelectromech. Syst.* **26**, 143–157 (2017).
86. J. Hong et al., "Continuous color reflective displays using interferometric absorption," *Optica* **2**, 589 (2015).
87. S. J. Cartamil-Bueno et al., "Graphene mechanical pixels for interferometric modulator displays," *Nat. Commun.* **9**, 4837 (2018).
88. B. Gally et al., "5.1: invited paper: a 5.7 color mirasol XGA display for high performance applications," in *SID Symp. Digest of Tech. Pap.*, Vol. 42, pp. 36–39 (2011).
89. F. Jutzi et al., "Low voltage electrostatic 90° turning flap for reflective MEMS display," in *Int. Conf. Opt. MEMS and Nanophotonics*, IEEE (2010).
90. F. Jutzi, W. Noell, and N. F. de Rooij, "Vertical electrostatically 90° turning flaps for reflective MEMS display," *Proc. SPIE* **7930**, 79300H (2011).
91. D. Herle et al., "Broadband mechanically tunable metasurface reflectivity modulator in the visible spectrum," *ACS Photonics* **10**(6), 1882–1889 (2023).
92. S. K. Cho, H. Moon, and C.-J. Kim, "Creating, transporting, cutting, and merging liquid droplets by electrowetting-based actuation for digital microfluidic circuits," *J. Microelectromech. Syst.* **12**, 70–80 (2003).
93. J. Li et al., "Current commercialization status of electrowetting-on-dielectric (EWOD) digital microfluidics," *Lab Chip* **20**(10), 1705–1712 (2020).
94. B. J. Feenstra, R. A. Hayes, and M. W. J. Prins, "Display device," US Patent 7,898,718 (2011).
95. R. A. Hayes and B. J. Feenstra, "Video-speed electronic paper based on electrowetting," *Nature* **425**, 383–385 (2003).
96. F. Mugele and J.-C. Baret, "Electrowetting: from basics to applications," *J. Phys. Condens. Matter* **17**, R705–R774 (2005).
97. IEEE Spectrum, "The electrowetting display," (2013). https://www.youtube.com/watch?v=Bf1GjCaYzYg (accessed 25 September 2023).
98. M. Zhou et al., "Simplified dynamical model for optical response of electrofluidic displays," *Displays* **49**, 26–34 (2017).
99. E. M. Barston, "Comments on 'electrohydrodynamic Rayleigh-Taylor bulk instability'," *Phys. Fluids* **13**, 2876–2878 (1970).
100. L. Wang et al., "Driving scheme optimization for electrowetting displays based on contact angle hysteresis to achieve precise gray-scales," *Front. Phys.* **9**, 655547 (2021).
101. F. Li and F. Mugele, "How to make sticky surfaces slippery: contact angle hysteresis in electrowetting with alternating voltage," *Appl. Phys. Lett.* **92**, 244108 (2008).
102. Y.-C. Chen et al., "56.3: a charge trapping suppression method for quick response electrowetting displays," in *SID Symp. Digest of Tech. Pap.*, Vol. 41, p. 842 (2010).
103. J. R. Platt, "Electrochromism, a possible change of color producible in dyes by an electric field," *J. Chem. Phys.* **34**, 862–863 (1961).
104. S. K. Deb, "A novel electrophotographic system," *Appl. Opt.* **8**, 192 (1969).
105. J. Svensson and C. Granqvist, "Electrochromic tungsten oxide films for energy efficient windows," *Sol. Energy Mater.* **11**, 29–34 (1984).
106. C. M. Lampert, "Electrochromic materials and devices for energy efficient windows," *Sol. Energy Mater.* **11**, 1–27 (1984).
107. C. M. Lampert, "The world of large-area glazing and displays," *Proc SPIE* **3788** (1999).
108. C. Lampert, "Large-area smart glass and integrated photovoltaics," *Sol. Energy Mater. Sol. Cells* **76**, 489–499 (2003).

109. A. M. Österholm et al., "Four shades of brown: tuning of electrochromic polymer blends toward high-contrast eyewear," *ACS Appl. Mater. Interfaces* **7**, 1413–1421 (2015).
110. Y. Wang et al., "Pulsed electrochemical deposition of porous WO3/sub on silver networks for highly flexible electrochromic devices," *J. Mater. Chem. C* **7**(7), 1966–1973 (2019).
111. H. Yu et al., "Side-chain engineering of green color electrochromic polymer materials: toward adaptive camouflage application," *J. Mater. Chem. C* **4**(12), 2269–2273 (2016).
112. N. O. Laschuk et al., "Post-synthetic color tuning of the ultra-effective and highly stable surface-confined electrochromic monolayer: shades of green for camouflage materials," *ACS Appl. Mater. Interfaces* **13**(33), 39573–39583 (2021).
113. C. R. Wade, M. Li, and M. Dincă, "Facile deposition of multicolored electrochromic metal-organic framework thin films," *Angew. Chem. Int. Ed.* **52**, 13377–13381 (2013).
114. Y.-M. Zhang et al., "A single-molecule multicolor electrochromic device generated through medium engineering," *Light Sci. Appl.* **4**, e249–e249 (2015).
115. L. Niklaus et al., "Redox electrolytes for hybrid type II electrochromic devices with fe-MEPE or nisub1-ix/i/subo as electrode materials," *ChemElectroChem* **7**, 3274–3283 (2020).
116. S. Bogati, A. Georg, and W. Graf, "Sputtered Si_3N_4 and SiO_2 electron barrier layer between a redox electrolyte and the WO_3 film in electrochromic devices," *Sol. Energy Mater. Sol. Cells* **159**, 395–404 (2017).
117. S. Bogati, R. Basnet, and A. Georg, "Iridium oxide catalyst for hybrid electrochromic device based on tetramethylthiourea (TMTU) redox electrolyte," *Sol. Energy Mater. Sol. Cells* **189**, 206–213 (2019).
118. Y. Wang et al., "A multicolour bistable electronic shelf label based on intramolecular proton-coupled electron transfer," *Nat. Mater.* **18**, 1335–1342 (2019).
119. X. Wang et al., "Reversible bond/cation-coupled electron transfer on phenylenediamine-based rhodamine b and its application on electrochromism," *ACS Appl. Mater. Interfaces* **9**(23), 20196–20204 (2017).
120. H. Shin et al., "Energy saving electrochromic windows from bistable low-HOMO level conjugated polymers," *Energy Environ. Sci.* **9**(1), 117–122 (2016).
121. T. S. Hernandez et al., "Bistable black electrochromic windows based on the reversible metal electrodeposition of Bi and Cu," *ACS Energy Lett.* **3**(1), 104–111 (2017).
122. S. Zhang et al., "$AlSuP_3$/ sup intercalation/de-intercalation-enabled dual-band electrochromic smart windows with a high optical modulation, quick response and long cycle life," *Energy Environ. Sci.* **11**(10), 2884–2892 (2018).
123. Z. Sun and Y. Fang, "Fabry-Pérot interference cavity length tuned by plasmonic nanoparticle metasurface for nanophotonic device design," *ACS Appl. Nano Mater.* **3**, 10732–10738 (2020).
124. M. Gugole et al., "Electrochromic inorganic nanostructures with high chromaticity and superior brightness," *Nano Lett.* **21**(10), 4343–4350 (2021).
125. T. Xu et al., "High-contrast and fast electrochromic switching enabled by plasmonics," *Nat. Commun.* **7**(1), 10479 (2016).
126. B.-H. Chen et al., "Printed multicolor high-contrast electrochromic devices," *ACS Appl. Mater. Interfaces* **7**, 25069–25076 (2015).
127. K. Xiong et al., "Electronic paper: plasmonic metasurfaces with conjugated polymers for flexible electronic paper in color (adv. mater. 45/2016)," *Adv. Mater.* **28**, 10103–10103 (2016).
128. N. Kobayashi et al., "Organic electrochromism for a new color electronic paper," *Sol. Energy Mater. Sol. Cells* **92**, 136–139 (2008).
129. T. Yashiro et al., "Flexible electrochromic display," in *Proc. IDW*, Vol. 13, pp. 1300–1303 (2013).
130. S. I. Cho et al., "Nanotube-based ultrafast electrochromic display," *Adv. Mater.* **17**(2), 171–175 (2005).
131. M. Wuttig, "Towards a universal memory?" *Nat. Mater.* **4**, 265–266 (2005).
132. H. Bhaskaran and P. Hosseini, "Display device based on phase-change materials," US Patent 9,823,538 (2017).
133. C. Koch et al., "Investigating the influence of resonant bonding on the optical properties of phase change materials (GeTe)subix/i/subSnSbsub2/subsesub4/sub," *Chem. Mater.* **29**, 9320–9327 (2017).
134. S. R. Ovshinsky, "Reversible electrical switching phenomena in disordered structures," in *Disordered Materials*, pp. 11–13, Springer US (1991).
135. E. Ohno et al., "TeGeSnAu alloys for phase change type optical disk memories," *Jpn. J. Appl. Phys.* **28**, 1235 (1989).
136. P. Hosseini, C. D. Wright, and H. Bhaskaran, "An optoelectronic framework enabled by low-dimensional phase-change films," *Nature* **511**, 206–211 (2014).
137. M. A. Kats et al., "Nanometre optical coatings based on strong interference effects in highly absorbing media," *Nat. Mater.* **12**(1), 20–24 (2013).
138. K. Shportko et al., "Resonant bonding in crystalline phase-change materials," *Nat. Mater.* **7**, 653–658 (2008).
139. B. Broughton et al., "38-4: solid-state reflective displays (SRD) utilizing ultrathin phase-change materials," in *SID Symp. Digest of Tech. Pap.*, Wiley Online Library, Vol. 48, pp. 546–549 (2017).

140. S. G. Castillo et al., "57-4: solid state reflective display (SRD) with LTPS diode backplane," in *SID Symp. Digest of Tech. Pap.*, Wiley Online Library, Vol. 50, pp. 807–810 (2019).
141. O. Hemmatyar et al., "Advanced phase-change materials for enhanced meta-displays," arXiv:2105.01313 (2021).
142. T. Zhou et al., "Electrically tunable non-volatile reflective display pixel structure based on phase change material," *J. Phys. Conf. Ser.* **1544**, 012034 (2020).
143. E. Yablonovitch, "Inhibited spontaneous emission in solid-state physics and electronics," *Phys. Rev. Lett.* **58**(20), 2059 (1987).
144. S. John, "Strong localization of photons in certain disordered dielectric superlattices," *Phys. Rev. Lett.* **58**(23), 2486 (1987).
145. Z. A. Zaky and A. H. Aly, "Novel smart window using photonic crystal for energy saving," *Sci. Rep.* **12**, 10104 (2022).
146. H. Wang and K.-Q. Zhang, "Photonic crystal structures with tunable structure color as colorimetric sensors," *Sensors* **13**(4), 4192–4213 (2013).
147. G. A. Ozin and A. C. Arsenault, "P-ink and elast-ink from lab to market," *Mater. Today* **11**(7-8), 44–51 (2008).
148. I. Lee et al., "Quasi-amorphous colloidal structures for electrically tunable full-color photonic pixels with angle-independency," *Adv. Mater.* **22**(44), 4973–4977 (2010).
149. C. Jin et al., "Photonic gap in amorphous photonic materials," *Phys. Rev. B* **63**(19), 195107 (2001).
150. K. Ueno et al., "A soft glassy colloidal array in ionic liquid, which exhibits homogeneous, non-brilliant and angle-independent structural colours," *Chem. Commun.* (24), 3603–3605 (2009).
151. Y. Fang et al., "In situ dynamic study of color-changing in liquid colloidal crystals for electrophoretic displays," *ACS Appl. Nano Mater.* **5**(8), 11249–11261 (2022).
152. G. Chen et al., "Development of bright and low angle dependence structural colors from order-disorder hierarchical photonic structure," *Dyes Pigments* **161**, 464–469 (2019).
153. N. Vogel et al., "Color from hierarchy: diverse optical properties of micron-sized spherical colloidal assemblies," *Proc. Natl. Acad. Sci.* **112**(35), 10845–10850 (2015).
154. K. Werner, "La chapter's one-day conference covers North American display activity," *Inf. Disp.* **35**(4), 34–36 (2019).
155. M. Wang et al., "59.1: invited paper: electrophoretic display platform comprising b, w, r particles," in *SID Symp. Digest of Tech. Pap.*, Wiley Online Library, Vol. 45, pp. 857–860 (2014).
156. W. Markvoort, H. E. A. Huitema, and L. M. Hage, "Sequential addressing of displays," US Patent 8,866,733 (2014).
157. E ink epaper ED103TC2, https://www.data-modul.com/sites/default/files/products/VB3300-KCD-specification-12051789.pdf (accessed 2 April 2024).
158. R. Fleming et al., "48-2: electronic paper 2.0: frustrated eTIR as a path to color and video," in *SID Symp. Digest of Tech. Pap.*, Wiley Online Library, Vol. 49, pp. 630–632 (2018).
159. A. Khan et al., "Recent advances and product enhancements in reflective cholesteric displays," *Proc. SPIE* **5741**, 1–6 (2005).
160. D. Corr et al., "Coloured electrochromic "paper-quality" displays based on modified mesoporous electrodes," *Solid State Ionics* **165**(1–4), 315–321 (2003).
161. I. J. Ko et al., "An optically efficient full-color reflective display with an electrochromic device and color production units," *J. Inf. Disp.* **20**, 155–160 (2019).
162. M. Z. Duan et al., "A reflective display technology based on electrofluidics," *Appl. Mech. Mater.* **670**, 976–981 (2014).
163. S. Wilson and M. Hutley, "The optical properties of 'moth eye' antireflection surfaces," *Optica Acta: Int. J. Opt.* **29**(7), 993–1009 (1982).
164. T. Yano, H. Sugawara, and J. Taniguchi, "Moth-eye structured mold using sputtered glassy carbon layer for large-scale applications," *Micro Nano Eng.* **9**, 100077 (2020).
165. H. K. Raut et al., "Anti-reflective coatings: a critical, in-depth review," *Energy Environ. Sci.* **4**(10), 3779–3804 (2011).
166. "The new re monitor by SVD: Our 32" RLCD with more connectivity," Sun Vision Display, a TM Brand of New Vision Display, https://www.sunvisiondisplay.com/product/The-NEW-rE-Monitor-Featuring-32-Color-RLCD-Technology (accessed 2 April 2024).
167. G. Hong et al., "A brief history of OLEDs—emitter development and industry milestones," *Adv. Mater.* **33**(9), 2005630 (2021).
168. H. Alex et al., "Introduction of a new disruptive display technology in the existing display manufacturing infrastructure," in *Proc. Int. Disp. Workshops*, p. 739 (2020).
169. J. Heikenfeld et al., "Electrofluidic displays using young–Laplace transposition of brilliant pigment dispersions," *Nat. Photonics* **3**(5), 292–296 (2009).
170. M. Jin et al., "Optofluid-based reflective displays," *Micromachines* **9**(4), 159 (2018).

171. C. Gu et al., "Emerging electrochromic materials and devices for future displays," *Chem. Rev.* **122**(18), 14679–14721 (2022).
172. Q. Fu et al., "Electrically responsive photonic crystals with bistable states for low-power electrophoretic color displays," *Nat. Commun.* **13**(1), 7007 (2022).
173. L. Whitehead, "Total internal reflection for illumination and displays," SPIE Newsroom, https://spie.org/news/0461-total-internal-reflection-for-illumination-and-displays (2006).

Dorian Herle is a PhD student at École Polytechnique Fédérale de Lausanne (EPFL), Switzerland. He received his MSc degree in mechanical engineering from EPFL in 2019. His current research focuses on MEMS-based tunable metasurfaces.

Olivier J. F. Martin conducts comprehensive research that combines the development of numerical techniques, advanced nanofabrication, and experiments on plasmonic systems. Applications of his research include optical antennas, metasurfaces, nonlinear optics, optical nano-manipulations, heterogeneous catalysis, security features, and optical forces at the nanoscale. He has authored over 300 journal articles and holds several patents and invention disclosures.

Luis Guillermo Villanueva is an associate professor at École Polytechnique Fédérale de Lausanne, Switzerland, where he specializes in NEMS/MEMS sensing technologies. He received his MSc degree in physics from Zaragoza and his PhD from UAB in Barcelona. He has contributed over 100 papers to peer-reviewed journals. He has served on program committees for major conferences including IEEE-NEMS and IEEE-Sensors and is the editor-in-chief of the Physical Sensors Section of *MDPI Sensors*.

Niels Quack is an associate professor at the University of Sydney, Australia. He received his MSc degree from Ecole Polytechnique Fédérale de Lausanne (EPFL), Switzerland, in 2005, and his Dr.Sc. degree from ETH Zürich, Switzerland, in 2010. He was a postdoctoral researcher at UC Berkeley, United States, from 2011 to 2015 and assistant professor at EPFL from 2015 to 2021. His research focuses on photonic micro- and nanosystems. He is senior member of IEEE and of Optica and a life member of SPIE.